THE DYNAMIC BEHAVIOUR OF MILD STEEL

THE DYNAMIC BEHAVIOUR

OF

MILD STEEL

BY

MICHAEL A. BURKE, B.Sc., B.Eng.

A Thesis

Submitted to the School of Graduate Studies

in Partial Fulfillment of the Requirements

for the Degree

Master of Engineering

McMaster University

May, 1970

MASTER OF ENGINEERING (1970)
(Mechanical Engineering)

McMASTER UNIVERSITY
Hamilton, Ontario.

TITLE: The Dynamic Behaviour of Mild Steel

AUTHOR: Michael Anthony Burke, B.Sc. (Loyola College)
B.Eng. (McGill University)

SUPERVISOR: Dr. G. Kardos

NUMBER OF PAGES: xii, 123

SCOPE AND CONTENTS:

Multiple impact tests were performed on mild steel. The pulse durations ranged from 15 to 250 milliseconds. Peak stresses extending to 135,000 p.s.i. were attained.

A dynamic model, based on dislocation dynamics, was derived for polycrystalline metals and made specific to mild steel. The model provided a means of indirectly determining the dislocation velocity-stress exponent n by experiment.

An empirical flow function was evaluated which related dynamic load conditions to plastic deformation. This function is a further extension of the dynamic model. Several dislocation parameters are grouped together to permit experimental evaluation of the strain rate effect on crystalline material.

Experimental studies indicated that a given strain:

1) if produced by a single pulse, can be estimated by evaluation

of the flow function for that load-time trace, or,

2) if produced by multiple impacts, can be estimated by the cumulative flow function, a summation of the flow functions for all impact traces.

The multiple impact tests established the flow function as an equation of state. The plastic deformation could then be determined for a given dynamic load as long as the strain history is known.

The theoretical model was used to support the experimental findings.

ACKNOWLEDGEMENTS

Sincere appreciation is due Dr. G. Kardos of the Mechanical Engineering Department of this University, who supervised the research efforts described in this paper. His contribution to the evolution of a design criterion for the dynamic behaviour of metals has been a stimulus for continued experimental work in this area. His guidance and suggestions have been most helpful. Financial support was provided by National Research Council Grant Number A3340 which was awarded to Dr. Kardos.

The author is grateful to Dr. J.D. Embury and Mr. D. Timbres of the Metallurgy Department who permitted the use of heat treatment facilities of that department for the purpose of annealing the specimens.

Appreciation is also due Mr. J. Meyers of the Civil Engineering Department and Mr. B. Williams of the Electrical Engineering Department who kindly assisted in the maintenance and repair of the experimental apparatus.

The author is also grateful to Messrs. L. Galloway and F. Boehm of Westinghouse (Hamilton Plant No.2) for the use of their optical comparator.

The author expresses his thanks to Mrs. L. Mazur and Mrs. C. Burke who typed this thesis.

TABLE OF CONTENTS

TABLE OF CONTENTS (CONTINUED)

LIST OF ILLUSTRATIONS

LIST OF ILLUSTRATIONS (CONTINUED)

LIST OF ILLUSTRATIONS (CONTINUED)

LIST OF TABLES

NOTATION

a	=	Dislocation multiplication exponent
A_1	=	Specimen cross-sectional area
A_2	=	Load piston cross-sectional area
A_3	=	Drive piston cross-sectional area
b	=	Burger's vector
B	=	Fluid bulk modulus
c	=	Peak stress - strain constant
C	=	Dislocation multiplication parameter
D	=	Empirical force - drop height constant
$\epsilon_p, \epsilon_t, \epsilon_r$	=	Plastic, cumulative, residual strain
$E\ (t)$	=	Error function
f	=	Mobile fraction of total dislocation density
$f\ (\phi)$	=	Non-dimensional stress variable
$G\ (\epsilon_r, t_o)$	=	Flow function - including strain hardening
H	=	Drop height
$H\ (\epsilon_r)$	=	Flow function - without strain hardening
k	=	Dislocation generating coefficient
$K\ (n)$	=	Pulse form function
L_1	=	Length of specimen
m	=	Geometric strain progression exponent
M	=	Mass of drop table
n	=	Dislocation velocity - stress exponent
N_o^*, N^*	=	Initial, average mobile dislocation density

p	=	Empirical force - drop height constant
q	=	Linear strain hardening coefficient
r	=	Geometrical progression factor
R	=	Slope of ramp load - time pulse
S	=	Peak stress - strain constant
t_o, t_D	=	Pulse duration, yield delay time
U	=	Potential energy of a deflected spring
v, v^*	=	Average dislocation velocity, terminal velocity
V	=	Volume of intensifier
W	=	Upper yield stress - strain rate constant
x	=	Average dislocation displacement in a unit volume
y	=	Drive piston displacement
Y	=	Modulus of elasticity
θ	=	Angle between normal to glide plane and stain axis
λ	=	Angle between average glide direction and strain or stress axis
ϕ	=	Non-dimensional time variable
η	=	Orientation factor
ψ	=	Dislocation mobility coefficient
γ	=	Plastic shear strain
τ	=	Applied shear stress
π	=	Critical density of dislocations
Γ	=	Spring constant of intensifier
σ, σ_m, $\sigma_{U.Y.}$, $\sigma_{L.Y.}$, σ^*	=	Applied compressive stress, nominal peak, upper dynamic yield, lower dynamic yield, yield stress at 0^oK.

NOTATION (CONTINUED)

σ_o, τ_o	=	Direct, shear stress producing unit dislocation velocity

CHAPTER 1

INTRODUCTION

1.1 Multiple Impacts

The first experimental studies in the dynamic behaviour of materials under repeated impacts were performed by Campbell[26]. The objective was to obtain improved dynamic stress-strain diagrams. Prior to these experiments, the diagrams were obtained from a number of tests on different specimens at various impact velocities. Each test produced a single point on the stress-strain diagram representing the peak stress and strain achieved at a given velocity. Repeated impacts on the same specimen eliminated scatter in the stress-strain diagram due to the variation among specimens.

Kolsky[25] performed multiple impact tests in an attempt to describe the variation of permanent strain with the number of impacts on a material. The impact velocity remained constant for each test. It was assumed that in specimens that had yielded, the material would behave elastically up to the peak stress to which it had previously been subjected. Knowing the dynamic stress-strain curve for the material, a new stress-strain curve could be established for the deformed specimen by making use of the assumption discussed above. A relationship

was then established between impact velocity and permanent strain based on the theory of plastic wave propagation. The experimental results differed greatly from the theoretical predictions.

Clark[16] discusses multiple impact tests where the effect on delay-yield time was examined as a result of pre-loading specimens at a constant stress level.

In the multiple impact experiments discussed in this paper, an empirical function was established as an equation of state. By means of this function, the deformation of a specimen could be predicted for a dynamic load condition as long as the strain history is known. The derivation of this function is based on the theory of dislocation dynamics.

1.2 Dislocation Dynamics

The theory of dislocation dynamics has synthesized the various branches of the knowledge of dislocations. This new phenomenological theory of plasticity, based on the study of mobile dislocations, can be used for mechanical design purposes and as a framework for further theoretical advances. Material deformation behaviour can now be predicted from a knowledge of its dislocation parameters.

Experimental dislocation dynamics had its origin in the measurement of the properties of individual dislocations by Johnston and Gilman[1] in 1959. They demonstrated that when the applied stress is sufficiently high so as to cause dislocation motion, profuse

dislocation nucleation and multiplication occur. Prior to these observations of dislocation behaviour, emphasis had been placed on static effects, such as Cottrell pinning or the stress to operate a Frank-Read source, as factors that determine the yielding of crystals. It is now evident that it is the dynamic resistance to dislocation motion in a crystal that determines the yield stress. Macroscopic plastic flow depends on the number of mobile dislocations and their velocity. Measurements of these quantities are now available.

A consistent theory has been developed from dislocation dynamics that readily accounts for many phenomena associated with the mechanical testing of materials. This theory explains some of the macroscopic phenomena associated with yielding. Hahn[2,3] derived a model for yielding based on dislocation multiplication and velocity characteristics that describes yield points, abrupt yield drop, yield delay time, Lüders band front velocity, and strain rate sensitivity for iron and other related body centered cubic metals. This model has also been extended to describe fracture. The influence of deformation parameters on the response of materials to a running crack, has been calculated.

1.3 Design Criteria

The mathematical model derived by Hahn to describe the dynamic response of metallic materials requires the knowledge of several constants. These constants appear in expressions for the mobility and multiplication of dislocations in a material at a specific state and for a given

temperature. The values of the constants have been determined experimentally for only a few materials and are accurate only to the order of their magnitude. Consequently, the model can only be used in a qualitative manner. Kardos[4] in establishing a design criterion proposed a specific form of the model that grouped the constants together into a quasi-single valued function of residual strain. This *flow function* is evaluated empirically along with an index relating applied stress to dislocation velocity for that material. The deformation behaviour of any material can then be predicted for a known dynamic loading condition using the two empirical values.

The design relations are applicable to materials that react to dynamic loading in the manner described by the microdynamical theory of plasticity. This theory employs empirical relations to equate microscopic entities to macroscopic observations.

The experiments discussed in this paper were performed on mild steel specimens. The constant n appearing in the dislocation velocity-shear stress equation was evaluated by indirect methods. The dislocation velocity can be readily approximated by a power function of the applied shear stress,

$$v = \left(\frac{\tau}{\tau_0} \right)^n \qquad (1)$$

The flow function was then calculated for a specific load pulse as follows:

$$G\ (\varepsilon_r, t_o) = \sigma_m^n\ t_o\ K(n) \qquad (2)$$

where $K(n)$ is a form function describing the pulse shape. The value

of $G(\varepsilon_r, t_o)$ was then plotted against strain providing an equation of state for the material. The validity of this strain function was examined by first constructing the curve from a series of single impact tests. Specimens were then loaded repeatedly and the cumulative flow function was plotted against residual strain. The collapsing of the multiple impact results on to the single impact curve validated the use of $G(\varepsilon_r, t_o)$ vs. ε_r as an equation of state. Thus, the strain ε_r for a given flow function G_T can be the result of a single dynamic pulse or several impacts where

$$G_T = G_1 + G_2 + \ldots\ldots\ldots\ldots + G_n \qquad (3)$$

The resulting plastic strain in the latter instance would be the sum of the incremental strains for each pulse.

Two qualifications must be made regarding the empirical flow function:

1) The flow function is valid for a fixed region of plastic strain and a fixed range of applied stress. The region of plastic strain is that within which the dislocation multiplication expression is valid. The stress must be in the range for which the dislocation mobility relation, stated above, is applicable, and,

2) The flow function in actual fact is not solely dependent on the residual strain, but is also a function of the pulse duration and shape. This is apparent as a result of computer experiments performed by Kardos[4] using the model equation that describes the

yield mechanism of crystalline solids. However, this empirically derived function when employed as a quasi-single valued function can provide conservative design estimates regarding the deformation of a structure.

In the following chapter, the theory of dislocation dynamics will be examined and a model for the dynamic behaviour of mild steel will be proposed. From this model, the author has derived expressions that suggest an indirect method of experimentally determining the value of n. The derivation of the flow function will be reviewed. This function provides a relation between the dynamic load condition and the resultant plastic deformation for a specific material.

Chapter 3 describes the experimental apparatus and procedures for performing the tests, as well as an analysis of the response of the system. The results of the experiments are discussed in Chapter 4 of this paper. The principal considerations were the evaluation of the dislocation velocity-stress exponent and the relation between the cumulative flow function and the residual strain. Other areas of investigation include the variation of peak stress and residual strain with successive impacts and, the variation of residual strain with peak elastic stress. Chapter 5 describes the results of numerical studies using the mathematical model established in Chapter 2 to support the experimental findings given in Chapter 4.

CHAPTER 2

THEORY

2.1 Introduction

The mathematical model derived by Hahn[2] and extended by Kardos[4] to describe the dynamic behaviour of mild steel, is semi-empirical in form. The mobility and density of dislocations are related to the macroscopic stress and strain by means of empirical constants. The following section provides further insight into the microdynamical theory upon which the dynamic model is based.

2.2 Microscopic Equation

For a theory to predict macroscopic behaviour, it is necessary to be able to express the microscopic variables that determine the rate at which plastic flow occurs by means of the motions of dislocation lines, in terms of the macroscopic stress and strain. Three microscopic variables are involved: the mean dislocation velocity, v, the mean density of mobile dislocations N^* and the Burgers vector b, a measure of the magnitude and direction of a dislocation.

The macroscopic plastic shear strain in a single crystal is

given by:

$$\gamma = b N^* x \qquad (4)$$

where x is the average distance moved by a dislocation through a unit volume of a crystal. The plastic strain rate is therefore

$$\dot{\varepsilon}_p = \eta b N^* v \qquad (5)$$

where v is the average velocity of a dislocation. The factor η is a geometrical one relating the microscopic flow to the macroscopic flow direction. It equals $\cos\theta \cos\lambda$ where λ is the angle between the average glide direction and the macroscopic strain axis and θ is the corresponding angle for the normal of the average glide plane. For polycrystalline bodies, this factor will be $\cos^2\lambda$ where λ is the angle between the average glide direction in the aggregate and the principal stress direction. The angle λ is approximately 45 degrees and therefore, η will equal 0.5.

It shall be assumed, in accordance with the findings of Johnston and Gilman[1] that the dislocations in a material do not accelerate freely but, as in the case of lithium-fluoride crystals, travel with a well defined velocity. The general expression for plastic flow is made specific to a material by the insertion of the appropriate dislocation parameters, for that material, into equation 5.

The dislocation velocity-shear stress relationship for lithium-fluoride, illustrated in Figure 2, is considered as representative of

the stress dependence of dislocation velocity in mild steel.

By means of etch pits, the positions of dislocations can be found in a crystal before and after stress pulses of known amplitude and duration have been applied. Thus a Δx and Δt for a particular applied stress, can be determined, and curves of $v = \Delta x / \Delta t$ as a function of stress can be generated (Figure 2).

The nature of the velocity dependence on stress is revealed by plotting the logarithm of the velocity as a function of the reciprocal of the applied stress. A straight line results, as seen in Figure 3. Consequently, there exists a relation of the form

$$v = v^* e^{-\sigma_0 / \sigma} \qquad (6)$$

where v^* is the terminal velocity achieved when the applied stress σ becomes very great. The coefficient σ_0, having the dimensions of stress, is called the characteristic drag stress and is the dominant parameter. It is a material characteristic determined by such factors as the chemical structure of the crystal, the concentration of point defects (vacancies, interstitials, impurities), collisions with other dislocations, stacking faults, precipitates and grain boundaries.

A degenerate form of the dislocation velocity-stress relation can be obtained, if only a portion of the velocity spectrum, illustrated in Figure 2 a, is examined. If velocities below 100 centimetres per second are considered, or equivalently, shear stresses less than twice the yield stress, the velocity-stress relationship can

be expressed as:

$$v = \left(\frac{\sigma}{\sigma_o}\right)^n \tag{7}$$

The material characteristic, n, is a constant for a given temperature. The drag stress, σ_o, is that required to drive a dislocation with a unit velocity. Using equation 7 provides a more tractable dynamic model.

As a crystal is deformed plastically the internal structure changes in two significant ways.

First, the total dislocation density increases. It has been observed to be approximately, a linear function of strain. This is because dislocations are able to be generated, especially by means of the process of multiple cross-glide. As plastic flow progresses, new dislocations are created at a rate such that the increase in density is proportional to the density. Furthermore, it has been observed[1] that the rate will increase with the mean dislocation velocity. Consequently, the time rate of increase of dislocation density can be expressed as:

$$\dot{N}^* = k \; v \; N^* \tag{8}$$

where k is a generating coefficient. Substituting equation 8 into equation 5 yields upon integration

$$N^* = N_o^* + C \; \varepsilon_p \tag{9}$$

where $C = {}^{2k}/_{b}$

and N_o^* is the initial mobile density.

It is known that most annealed crystals possess a grown-in total dislocation density N_o, of about 10^6 to 10^8 cm/cm^3. However, when a crystal is stressed, most of the grown-in dislocations do not move; for example, they may have impurity particles precipitated along them or they may not lie parallel to glide planes. Only the mobile dislocations initially present, N_o^*, are available for flow. Gilman[20] states that heterogeneous nucleation is responsible for the majority of mobile dislocations that cause plastic flow in present day engineering materials. This nucleation is caused by concentrated stresses found near such heterogeneities as cracks, precipitates, and other defects in crystals. Figure 4 illustrates the experimental results of Hahn, Reid and Gilbert[3] depicting the rate of increase of total dislocation density with strain for mild steel. These curves can be described by equation 9, where the dislocation multiplication parameter C is of the order 2 - 4 x 10^9 cm/cm^3 per per cent strain. Figure 4 also illustrates the lack of sensitivity of this parameter to differing strain rates. No systematic change was found over a range of eight orders of magnitude. Similarly, Gilbert, Wilcox and Hahn[6] found that the total dislocation density in polycrystalline molybdenum increases by only a factor of 3 when the strain rate was increased by 10^8 sec^{-1}. The magnitude of C does seem to depend on the grain structure of the material; Keh and Weissman have found that an increase in grain size is accompanied by a decrease in the value of C. Reid[7]

has found a linear relation between C and the square root of grown-in dislocations, provided that the original density is in excess of about 10^4 cm/cm^3. Thus, it appears that the grown-in dislocations have an important role as obstacles, instrumental in determining the subsequent multiplication rate.

The second significant change in the internal structure of a plastically deforming crystal is the decrease in the ease of dislocation movement. This is due to the increasing frequency of dislocation interactions with increased plastic strain. This decrease in mobility can be described in two ways. The average dislocation velocity can be considered to decrease as a result of plastic strain, for a given applied stress. The drag stress would then become a function of plastic strain and would be expressed as:

$$\sigma_o \ (\varepsilon_p) = \sigma_o + q \ \varepsilon_p, \qquad (10)$$

where q is the rate of linear strain hardening.

The second way to describe the decrease in mobility is to consider that the mobile dislocations continue to move at the same speed, but the fraction of the total density that moves decreases continually with increasing strain. As straining proceeds, some of the dislocations given by equation 9 lose their mobility through interactions or become lost by emission from a surface. A factor f is then considered as the fraction of the total dislocation density that remains highly mobile. The fraction decreases with increasing strain. An increase in N^* leads to more interactions and thereby decreases f.

The factor f must also be dependent on the instantaneous mobile fraction itself because motion must occur if the fraction is to decrease. As a result,

$$d\ f \sim - f\ d\ N^*$$

but, from equation *9*,

$$d\ N^* \sim d\ \varepsilon_p$$

therefore,

$$d\ f = -\psi\ f\ d\ \varepsilon_p \qquad (11)$$

and upon integrating

$$f = e^{-\psi\ \varepsilon_p} \qquad (12)$$

Combining equation *12* with equation *9*, the mobile dislocation density is now expressed as:

$$N^* = (N_o^* + C\ \varepsilon_p)\ e^{-\psi\ \varepsilon_p} \qquad (13)$$

The form of this function is shown in Figure *5 c* while the individual factors are shown in Figures *5 a* and *5 b*. The rate of decrease in mobility with strain is lessened with an increase in stress. Therefore, the coefficient ψ will depend inversely on the stress and is given as:

$$\psi = \frac{q}{\sigma} \qquad (14)$$

A plastic strain rate equation based on the dislocation parameters listed in equation *5* can be derived by combining equations *6* and *13* and substituting into equation *5*. If the former method of describing decreasing dislocation mobility is employed, then equations *6*, *9* and *10* would be combined and substituted into equation *5*. The resulting macroscopic plastic strain rate model is given as:

$$\dot{\varepsilon}_p = 0.5b\ (N_o^* + C\ \varepsilon_p)\ v^*\ e^{-\left[\frac{\sigma_o + q\ \varepsilon_p}{\sigma}\right]} \qquad (15)$$

The dislocation velocity term in the above expression is

$$v = v^*\ e^{-\left[\frac{\sigma_o + q\ \varepsilon_p}{\sigma}\right]} \qquad (16)$$

The effects of work hardening have been included. As in the case of unstrained crystals, the above expression can be reduced to a degenerate form that is more manageable in a mathematical model. The result is

$$v = \left(\frac{\sigma}{\sigma_o + q\ \varepsilon_p}\right)^n \qquad (17)$$

This expression describes the linear relation, illustrated in Figure *2 b*, for strained crystals. The model equation may be expressed as:

$$\dot{\varepsilon}_p = 0.5b\ (N_o^* + C\ \varepsilon_p)\left(\frac{\sigma}{\sigma_o + q\ \varepsilon_p}\right)^n \qquad (18)$$

Hahn[2] derived an expression for the effect of work hardening on the velocity-stress relationship that is similar to equation *17*. In establishing the original mathematical model for dynamic yielding of mild steel, it was observed that the stresses associated with any given velocity are greater in a slightly deformed crystal than for

undeformed crystals. This fact is illustrated in Figure *3 b*. This increase in stress corresponds closely with the amount of work hardening displayed by the stress-strain curve. As a result, the effect of the applied stress is reduced by an amount equal to the work hardening increment. Gilman and Johnston[5] have demonstrated that the stress increment, $\Delta\sigma$, due to strain-hardening in lithium-fluoride is linearly related to the plastic strain. They have also remarked that the same mechanism of strain-hardening that occurs in lithium-fluoride may also operate in other crystals, since the same linear strain hardening effect has been observed in several metals. Consequently, the stress term appearing in equation *7* was replaced by the effective stress, where

$$\sigma_{eff.} = \sigma - \Delta\sigma \quad . \tag{19}$$

Modifying equation *7*, the velocity-stress relationship becomes

$$v = \left(\frac{\sigma - q\ \varepsilon_p}{\sigma_o} \right)^n \tag{20}$$

Hahn's model employed a non-linear expression to relate dislocation multiplication to plastic strain:

$$N^* = N_o^* + C\ \varepsilon_p^{\ a} \tag{21}$$

The dislocation multiplication exponent, a, has been calculated for various materials and varies in the range of 0.5 to 1.5. For mild steel, Hahn[3] found that a is approximately equal to unity. Consequently equation *21* is identical to equation *9*.

Combining equations *20* and *21* and substituting into equation *5*, the original dynamic model was given as:

$$\dot{\varepsilon}_p = 0.5b \left(N_o^* + C \varepsilon_p^a\right) \left(\frac{\sigma - q \varepsilon_p}{\sigma_o}\right)^n \qquad (22)$$

The velocity terms appearing in the dynamic models expressed in equations *18* and *22* are different. Both expressions are first approximations to the effect of work hardening on the velocity-stress relationship. At low values of plastic strain the expressions are approximately equal and both describe the shift in the velocity-stress curve for strained crystals, illustrated in Figure *2 b*.

2.3 Design Equation

A further macroscopic behaviour relationship was derived by Kardos[4], based on the dynamic model described in equation *22*. A flow function $H(\varepsilon_r)$ was established by re-arranging equation *22* and performing integration. The resulting expression was given as:

$$\int_o^{t_o} \left[\sigma(t) - q \varepsilon_p\right]^n dt = H(\varepsilon_r) \qquad (23)$$

The flow function is a material characteristic and solely dependent upon the residual strain. Most of the material constants are contained in this function. It is defined as:

$$H(\varepsilon_r) = \frac{\sigma_o^n}{0.5bN_o^*} \int_o^{\varepsilon_r} \frac{d\varepsilon_p}{(1 + C/N_o^* \varepsilon_p)} \qquad (24)$$

where ε_r is the residual strain resulting from a single stress pulse.

The left hand side of equation 23 can be expanded and re-written as:

$$\int_0^{t_o} \left[\sigma\ (t) - q\ \varepsilon_p\right]^n\ dt = \int_0^{t_o} \sigma\ (t)^n\ dt - \int_0^{t_o} E\ (t)\ dt \qquad (25)$$

The term $\int_0^{t_o} E\ (t)$ is a function of the form and duration of the load pulse, t_o. The design formula becomes:

$$\int_0^{t_o} \sigma\ (t)^n\ dt = H(\varepsilon_r) + \int_0^{t_o} E\ (t)\ dt \qquad (26)$$

The term on the right hand side may be grouped to produce a flow function, $G(\varepsilon_r, t_o)$, dependent upon both the residual strain and load pulse characteristics. Equation 23 can then be written as an equation of state:

$$\int_0^{t_o} \sigma\ (t)^n\ dt = G(\varepsilon_r, t_o) \qquad (27)$$

The left hand side of this equation can be expressed differently such that the effect of each of the loading parameters can be studied. The stress, a function of time, can be expressed in terms of its maximum value, σ_m, for a given pulse. The independent variable can be non-dimensionalized over the pulse duration.

Therefore,

$$\int_{o}^{t_o} \sigma\,(t)^{n}\,dt \;=\; \sigma_m^{n}\; t_o\; K(n) \qquad (28)$$

where $K(n)$ is called the form function. Equation 27 can be modified as:

$$\sigma_m^{n}\; t_o\; K(n) \;=\; G(\varepsilon_r,\, t_o) \qquad (29)$$

It can be deduced from the above expression that the flow function, for a given residual strain value, will increase directly with pulse duration and the area under the non-dimensionalized stress-pulse curve. However, for the purposes of a conservative design estimate of the dynamic loading effect on a structure, the flow function $G(\varepsilon_r,\, t_o)$, can be considered as a single valued function of the residual strain.

CHAPTER 3

EXPERIMENTAL PROGRAM

3.1 Apparatus

Figure *1* illustrates an assembly of the experimental equipment. The principal components are the drop table and the hydraulic intensifier, shown in Figure *6*.

The intensifier is a hydraulic fluid-filled chamber with an upper drive piston and a lower loading piston. A diagram of the intensifier is shown in Figure *7*. The fluid, having a bulk modulus of 18.4×10^4 pounds per square inch, is pumped into the intensifier. Simultaneously entrapped air is bled from the chamber through an air vent.

A controlled blow is imparted to the drive piston by means of the free falling drop table. The weight is released by remote control and is guided by runners in its fall. A pointer on the table indicates the drop height on a vertical scale. A latching mechanism brakes the drop table on its initial rebound so that the specimen has withstood only one load pulse. The downward displacement of the drive piston causes an increase in pressure in the chamber. The ratio of the loading piston area to that of the specimen is approximately 41.5, the factor

by which the intensifier pressure is multiplied to produce the applied stress.

The specimen is inserted between two anvils. The lower anvil rests on a Baldwin-Lima-Hamilton (Type C) strain gauge load cell. The load piston force is transmitted through the upper anvil to the specimen. The applied stress is therefore one of direct compression.

The signal produced by the load cell is amplified by means of a Tektronix Type 3C66 carrier amplifier and transmitted to a Tektronix Type 565 dual-beam oscilloscope. This signal is proportional to the applied force and the load cell excitation, which is provided by the amplifier. The oscilloscope trace is recorded on Polaroid Land Film Type 3000 by means of a Tektronix Type C-27 camera system. The single-sweep trace is triggered just before the falling weight impinges on the drive piston. The external triggering of the scope is accomplished by closing a circuit with a microswitch. A constant voltage source in the circuit overcomes a negative bias grid voltage on the scope. The microswitch located on the runner frame, is operated by means of a striker mounted on the drop table.

The intensifier was filled with hydraulic fluid by means of a hand pump. Fluid was pumped into the chamber until a bias pressure of 100 p.s.i. was achieved. Pressurizing the intensifier prevented any backlash of the system upon loading. The bias pressure was measured with a Type C Heise Gauge that was attached to the pump.

The polaroid photographs were assembled in series and re-photographed using a single 35 mm. film roll. The negative images were then projected using a Bausche and Lomb optical comparator with a 10 power magnification. The co-ordinates of each load pulse trace could then be measured. An average of 15 co-ordinates per trace was used for analytical purposes.

The specimens were measured before and after each load pulse with a Starrett Dial Indicator. The accuracy of this instrument is within .00005 inches.

Static compressive tests were performed on the material to obtain a stress-residual strain curve. A Tinius Olsen testing machine was used for this purpose. A pivotal head and base were used to insure that a direct compressive force was applied parallel to the longitudinal axis of the specimen; this permitted greater static stresses to be achieved before the inception of buckling. Each specimen was subjected to a series of load cycles, the maximum stress increasing with each cycle. Between each cycle the permanent strain was measured. The results were compared with those obtained for dynamic load cycles.

3.2 Specimens

The test pieces were cut and machined from a 5/8 inch diameter cold rolled mild steel rod. The final dimensions were:

Length: $1.5" \pm .001"$,

Diameter: $0.505" \pm .001"$

The ends were ground flat, parallel to each other and perpendicular to the surface.

The chemical analysis of the material was:

Carbon	.141%
Sulphur	.024%
Manganese	.43%

The specimens were heat treated in an evacuated atmosphere at 900 degrees Centigrade for a period of one hour. The material was then cooled to room temperature while remaining in the furnace. The purpose of the annealing was to provide a soft material, having a large average grain size in its microstructure, that would be very strain rate responsive. The specimens were heat treated in five batches due to the limitations in the furnace capacity. Three other methods of heat treatment were considered in an attempt to facilitate the annealing of a large quantity of specimens and to decrease the extent of oxidation of the specimen surface. Heat treatment by means of a salt bath and a technique by which the specimens were copper plated to prevent oxidation were examined. In addition, annealing in an inert gas atmosphere was also considered. In general, these methods, with the facilities used in the McMaster Metallurgical Department, did not produce a better specimen surface quality or improve the annealing of large quantities of specimens above that obtainable by the vacuum furnace.

Subsequent to heat treatment, the specimens were stored in a clear light hydraulic fluid in order to reduce the degree of surface oxidation. Prior to their use, the samples were cleaned with acetone

and alcohol solutions.

3.3 Load Variables

If the load piston deflection is assumed negligible in comparison to that of the drive piston, the response of the intensifier to an impact load is similar to that of a spring with a single degree of freedom. This assumption is valid in the case of elastically deforming specimens, where the strain-time pulse is proportional to the stress pulse. In cases where the elastic stress exceeds the dynamic yield stress of a specimen, the pulse is no longer sinusoidal, as a result of plastic deformation.

The induced stress function during loading is given as:

$$\sigma\ (t) = \frac{A_2}{A_1}\sqrt{\frac{B}{V}\ 2g\ HM}\quad sin\ A_3\sqrt{\frac{B}{VM}}\cdot t \qquad (30)$$

where

A_1 = specimen cross-sectional area

A_2 = load piston cross-sectional area

A_3 = drive piston cross-sectional area

V = volume of fluid in the intensifier

B = fluid bulk modulus

H = height of free fall of table

M = mass of drop table

Four of the variables listed in equation *(30)* are used to alter the load pulse characteristics with the available experimental equipment. They

are M, V, H and A_3. The bulk modulus, load piston and specimen size remained constant.

The variables are altered in fixed increments. The drop weight can be varied from 20 pounds to 250 pounds, using aluminum and steel tables of varying thickness. The intensifier volume can be varied by adding metal inserts to the chamber. The range extends from approximately 3 cubic inches to 120 cubic inches. The minimum drop height is governed by the space necessary to operate the drop table latch mechanism on rebound. This is about 2.5 inches. The maximum height is governed by the drop tester frame and it is 60 inches, however, this could be increased. Two drive pistons are available in order to vary the pulse duration. Their areas are 0.693 square inches and 0.2925 square inches. This permits the pulse duration to be increased by a factor of 2.37 with decreased drive piston area, for a given intensifier volume and drop table weight.

A smaller drive piston was designed for the experiments discussed in this paper in order to increase the pulse duration. The maximum pulse duration previously attained with the test apparatus was 90 milliseconds. It was estimated that by decreasing the area by a factor of 2.37, the pulse could be increased to approximately 215 milliseconds.

In the previous experiments performed with the apparatus, low pulse durations were achieved by inserting a large spacer into the intensifier chamber (See Figure *9*). The drive piston and spacer were

matched for an O-ring pressure fit. As the drive piston had no retainer, it was free to escape from the upper part of the intensifier under normal bias pressure or on rebound under loading conditions. To correct this situation, the inside diameter of the insert was increased, and small spacer rings of varying length were fitted loosely about the drive piston and retained by a ring attached to the end of this piston. As a result, normal bias pressures could be used and the piston was free to rebound on unloading without escaping from the intensifier. Also, small variations in intensifier volume could be achieved by adding or removing rings from around the drive piston.

Examination of the load pulse equation indicates that the form of the stress pulse is sinusoidal. The actual load-time trace will be a half sine wave, since the falling weight separates from the drive piston on rebound. It can be deduced that as the intensifier volume or drop weight increases, the applied frequency decreases and therefore, the pulse duration increases. A decrease in drive piston diameter also increases the time base, as discussed above. The amplitude of the stress pulse is given as:

$$\sigma_m = \frac{A_2}{A_1} \sqrt{\frac{B}{V} \; 2g \; HM} \quad , \qquad (31)$$

and for a given set of conditions for the intensifier, this term varies with the square root of the drop height of the table. From equation *(30)*, it can be seen that the amplitude of the stress pulse can be varied without altering the pulse duration.

By appropriate adjustment of the experimental apparatus variables, the dynamic yield stress for a specimen can be made to occur substantially below the peak elastic stress value. For a short pulse duration and large stress amplitude, the portion of the sinusoidal pulse up to dynamic yield can be approximated by a straight line. Consequently, the strain rate up to yield can be considered constant. Therefore, by varying the elastic stress amplitude the effect of strain rate on the upper dynamic yield stress can be studied.

Table *1* illustrates the variation in pulse duration with drive piston area, drop table weight and intensifier volume.

3.4 Calibration

The load cell output signal was calibrated, for a fixed excitation voltage, as a function of applied force. A measured force was applied to the cell by means of a static compression testing machine. The range extended to 45,000 pounds. An excitation voltage of 10.02 volts was applied using a constant d.c. voltage source. The output signal was detected using a very sensitive digital voltmeter. A linear relationship was found to exist between applied force and load cell output voltage. The load cell calibration factor was found to be 4×10^{-8} volts output per volt excitation, per pound applied force.

The amplifier-oscilloscope system was then calibrated as a unit. A constant d.c. millivolt source was applied, simulating the output signal from the load cell. The internal calibrating source of

the oscilloscope could not be used with the particular amplifiers employed in these experiments. The bandwidth of the amplifier was not sufficient to produce the square wave calibrating pulse. Consequently, a battery-potentiometer-resistor combination was placed in line with the inter-connecting cables from the amplifier. This arrangement produced the constant d.c. millivoltage.

The sensitivity of the amplifier is expressed in micro-strain per division and the excitation it produced across the leads to the load cell was measured as 2.5 volts. The calibration factor for the amplifier-scope system was found to be .00125 millivolts per micro-strain. A conversion factor can then be calculated for the entire system:

$$Force/Division = 12.5 \frac{lb.}{micro\text{-}strain} \times Sensitivity \quad \frac{micro\text{-}strain}{division} \qquad (32)$$

This factor was verified by applying a measured force with the static compression testing machine. The resulting oscilloscope trace deflection was observed.

The response of the drop tester and intensifier were examined using a fully hardened sample of the same dimensions as the test specimen. A typical load-time trace for the specimen that deforms only elastically is illustrated in Figure *8*. The trace begins at a positive constant value due to the bias pressure placed on the intensifier. As a result of the recoil of the entire system, the load on completion is seen to fall below the bias pressure. The oscillations seen at the end of the pulse are due to the ringing of the components of the intensifier.

Figure *8* verifies that the elastic response of the drop tester-intensifier unit is sinusoidal, the form being expressed by equation *(30)*.

Five pulse durations were used in the experiments, each time base resulting from a particular combination of intensifier volume and drop table weight. The peak force-drop height calibration was achieved for each pulse frequency, using the elastic or fully hardened specimen. The results were plotted on a log-log scale and found to be linear with values for the slopes in the range of 0.5. This relationship was predicted by equation *(31)*, where all the independent variables except H, the drop height, have been fixed for a specific time base. The calibrating relationship could then be expressed as:

$$Peak\ Force = D \times H^{p} \qquad (33)$$

where D and p are experimental constants and p approximates 0.5, the theoretical value. Figures *9* to *13* illustrate the calibrating curves for the five time bases used. The constants, D and p are given along with the correlation coefficient for the assumed linearity of the log-log plot. All values obtained were for a confidence level greater than 99%. Table *2* lists all the experimental constants that are involved.

The discrepancy between the experimental values of the peak force-drop height slope and the theoretically predicted value is due to the fact that the intensifier does not behave as a single spring but is in fact equivalent to a series of springs in its response. In addition to the displacement of the drive piston, there is some displacement in the load piston as a result of elastic deformation of the specimen and

a small deflection of the load cell. A rubber cap on the drive piston also deforms on impact.

The manner in which the drop table falls may also influence the response of the intensifier. The weight does not exactly drop in a free fall, but is guided by runners. Although these runners are set prior to dropping the weight so that a clearance exists with the frame, the guides are not perfectly straight and some caroming occurs, slowing the drop table slightly.

In some of the pulse traces, a very slight *kink* was observed in the rise portion of the loading, this indicates a slight striction in the drive piston collar. The latter two effects described above combine to produce a load pulse trace with values slightly less than those for a perfect sine pulse of the same amplitude and frequency.

The intensifier calibration was performed concurrent to the dynamic testing. The elastic specimen was subjected to a load pulse at the drop height and intensifier state that the subsequent *soft* sample would be tested. After a few samples had been tested at a particular pulse duration, a sketch was made of the calibrating curve in order to interpolate drop heights for subsequent tests so that the same range of elastic peak stress and strain would be examined as in the experiments at other pulse durations. Specifically, it was desired to maintain a constant range of plastic strain values, as a result of single load pulses. The range extended from 0.5% to approximately 6% in all pulse duration series with the exception of the 240 millisecond set of strains.

The effect of drive piston area on pulse duration was examined and compared to the theoretical prediction. For a drop table weight of 139 pounds and an intensifier volume of 120 cubic inches, a decrease in drive piston area by a factor of 2.37 caused an increase in pulse duration from 60 to 175 milliseconds, a 2.73 magnification. Using 250 pounds and the same volume, an increase from 90 to 243 milliseconds was obtained, a 2.7 magnification. The discrepancy between these values and the predicted 2.37 multiple is probably due to the non-linearities discussed above.

CHAPTER 4

EXPERIMENTAL RESULTS

4.1 Introduction

The tests were designed for a threefold purpose:

1) To examine the post-yield behaviour of mild steel specimens that were subjected to repeated dynamic loads. In particular, it was desired to examine the relation between the cumulative flow function and the resultant plastic strain after each successive impact.

2) To examine the dynamic yield behaviour of mild steel.

3) To determine, by indirect means, the exponent n relating dislocation velocity to applied dynamic stress. This constant is necessary for the determination of the empirical flow function relating load parameters to residual strain.

Forty specimens of the same material and heat treatment were tested. Five pulse durations were used, ranging from an average elastic time base of 14.6 milliseconds to 246.2 milliseconds (see

Table *1*). For a specific setting of the test apparatus variables, a specimen was subjected to several loading cycles. The period between loadings was ten minutes. The progression of plastic deformation under identical loading conditions was measured and the load-time trace for each cycle was recorded. Each specimen was re-loaded anywhere from two to twenty-four times. Multiple impacts continued until no observable change occurred in the load-time trace or until buckling occurred in the test pieces.

Figure *14* illustrates two typical load time traces. Each photograph contains two sets of curves and two curves per set. The upper set was monitored by the amplifier attached to the load cell; the lower set is obtained from a strain gauge attached to the outside wall of the intensifier. The sinusoidal curves are achieved in response to the load pulse being applied to the fully hardened specimen. The broken curves are obtained from the load application to the *soft* specimens. The onset of macroscopic yielding is characterized by a sudden decrease of load, as is particularly evident in Figure *14 b*. Figure *14 a* shows the effect on the plastic load-time trace, when the nominal peak stress (the maximum stress occurring in elastic deformation of the hardened sample) is almost equal to the dynamic yield stress of the material.

In cases where macroscopic yielding occurred, but no observable difference existed between the elastic and plastic load-time traces, the average residual strain was found to be 0.2% In

other cases where the ratio of dynamic yield stress to nominal peak stress was less than 0.75, the strain rate up to yield could be considered constant.

The range of strain rates experienced in the tests extended from .02 sec^{-1} to 1.0 sec^{-1}. This range could have been extended by utilizing the maximum available drop height, but the resulting strains were above those desired for the present study.

Figures *15* to *19* illustrate typical elastic and plastic responses for each of the five pulse durations that were used. It can be noted from these traces that the pulse duration, for specimens with significant plastic deformation, is longer than for purely elastic deformation at the same loading condition. Due to the plastic deformation of the specimen, the loading piston in the intensifier is displaced considerably. The displacement effectively increases the volume of the intensifier and from equation *30* it can be seen that the pulse duration will increase.

The data contained in each trace was reduced in the following manner:

A representative number of co-ordinates was measured using the optical comparator, each point having an X and Y length in inches. A conversion factor, $C.F.$, was established for both directions, relating comparator displacement to major divisions on the load-time trace. The stress value for a co-ordinate could then be determined:

$$Stress = 12.5 \frac{lb.}{micro\text{-}strain} \times Sens. \times Y \times C.F. \times \frac{1}{A_1} \qquad (34)$$

where

$Sens.$ = Sensitivity of amplifier ($^{micro\text{-}strain}/_{division}$)

Y = Comparator displacement in y direction (inches)

$C.F.$ = Comparator conversion factor (division/inches)

A_1 = Specimen cross sectional area (square inches)

In most cases, the flow function for a particular trace was desired. From equation *29* it is seen that the form function, $K\ (n)$ must be determined beforehand. It is defined as:

$$K\ (n) = \int_o^1 [f(\phi)]^n \ d\ \phi \qquad (35)$$

where $f\ (\phi)$ is a non-dimensional stress variable and ϕ is the non-dimensional time variable,

$$f\ (\phi) = \frac{\sigma}{\sigma_m} \qquad (36)$$

Figure *20* illustrates a plot of $f\ (\phi)$ and $[f\ (\phi)]^n$ against ϕ for the plastic load-time trace shown in Figure *16*. The area under the dashed curve represents the value of $K(n)$. It can be seen that the contribution of the area, beyond the range of 80% of the maximum stress value, is negligible and, therefore, the flow function can be accurately determined using only points within this range.

4.2 Dislocation Velocity

Tables *3* to *7* summarize the experimental results on all

specimens for a single pulse load. At the lower pulse durations of 14.6 ms., 36.6 ms., and 64.1 ms., the dynamic yield stress increases noticeably with peak stress or, equivalently, with strain rate. Alternatively, the yield stress decreases with an increase in time delay before yielding occurs.

Figure *21* is a log-log plot of yield stress dependence on strain rate. The resulting linear relationship can be described by the dynamic model.

The deformation accompanying the application of stress consists of an elastic and plastic part. However, at the upper or lower yield stress, in a material displaying a distinct yield drop, the elastic strain rate contribution $(^1/_Y \ d\sigma/dt)$ is zero. The constant Y is the elastic modulus. As a result, the total strain rate is given by equation *22*. At the yield point, where plastic strain is of the order of .1%, the effect of work hardening can be neglected. Equation *22* can then be written as:

$$\dot{\varepsilon}_p = constant \times \sigma^n_{U.Y.} \qquad (37)$$

where $\sigma_{U.Y.}$ is the upper yield stress.

Equation *37* provides an indirect means of experimentally determining the stress dependence of dislocation velocity. The log form of this equation is:

$$log \ \sigma_{U.Y.} = log \ W + {}^1/_n \ log \ \dot{\varepsilon}_p \qquad (38)$$

where $W = \sigma_o / (0.5\ b\ N_o^*)^{1/n}$

Consequently, the reciprocal of the value of the slope in Figure *21* is an estimate of the dislocation velocity exponent. The value of n determined in this manner was calculated as 19.68. The correlation coefficient for the apparent linear relationship illustrated is 0.93.

The stress dependence of delay time provides another means by which the velocity-stress parameter n can be determined indirectly. The delay time t_D, can be regarded as the time taken for a material under stress to deform to a minimum detectable yield strain, ε^*. Equation *22* can be integrated up to an observable yield time as follows:

$$\frac{\sigma_o^n}{0.5bN_o^*}\int_o^{\varepsilon^*} \frac{d\ \varepsilon_p}{\left[1 + \frac{C}{N_o^*}\ \varepsilon_p^a\right]} = \int_o^{t_D} \left[\sigma(t) - q\ \varepsilon_p\right]^n dt \qquad (39)$$

The pre-yield portion of the load-time traces can be approximated by a linear function,

$$\sigma = R \cdot t \qquad (40)$$

Neglecting the effect of work hardening in the low strain region and letting a equal unity, equation *39* can be expressed as:

$$\frac{(n+1)}{0.5\ b\ C}\ \sigma_o^n\ ln\ (1 + \frac{C}{N_o^*}\ \varepsilon^*) = R^n\ t_D^{n+1} \qquad (41)$$

Making use of equation *40*, this may be re-written as:

$$\sigma_y^n \; t_D = constant \qquad (42)$$

In log form, this becomes

$$log\ \sigma_{U.Y.} = \frac{-1}{n}\ log\ t_D + constant \qquad (43)$$

Figure *22* illustrates the log-log plot of yield stress against delay time. The value of n equals the absolute value of the reciprocal of the gradient; it is equal to 18.07. The correlation coefficient for the apparent linearity illustrated is 0.94.

It has been observed by Hahn and Gilbert[9] that the slope n increases slightly with strain rate and stress. This becomes evident, when the basic strain rate equation is examined. Expressing equation *5* in log form and differentiating with respect to the logarithm of applied stress, the expression becomes:

$$\frac{\partial\ log\ \dot{\epsilon}_p}{\partial\ log\ \sigma} = \frac{\partial\ log\ N^*}{\partial\ log\ \sigma} + \frac{\partial\ log\ v}{\partial\ log\ \sigma} \qquad (44)$$

If n' is considered as the experimentally determined approximation to n, this equation becomes:

$$n' = \frac{\partial\ log\ N^*}{\partial\ log\ \sigma} + n \qquad (45)$$

It has been observed in experiments with molybdenum[6] and chromium[10] that the term ($\partial\ log\ N^* /\ \partial\ log\ \sigma$) is positive but that its value tends to zero as the plastic strain approaches zero.

Therefore, the value of n' determined by means of equation *38* should closely approximate a value of n obtained by direct observation of etch-pits.

The variation of mobile dislocation density with strain rate effects the approximate value of n. Equation *5* can be written in the form:

$$1 = \frac{\partial \log N^*}{\partial \log \dot{\varepsilon}_p} + n \frac{\partial \log \sigma_y}{\partial \log \dot{\varepsilon}_p} \qquad (46)$$

From Figure *4* it is noted that the dislocation density at any plastic strain is about a factor of two greater for tests carried out at a strain rate of 2×10^{-2} sec^{-1} than for tests at 2×10^{-5} sec^{-1}. Thus, the term $(\partial \log N^* / \partial \log \dot{\varepsilon}_p)$ is negligible and the log-log plot of strain rate variation with yield stress, provides a close approximation to n.

For load pulses where the residual strain is extremely small, approaching the yield point strain of .1%, the work hardening term in equation *23* can be neglected. As a result, the equation becomes:

$$\int_o^{t_o} \sigma (t)^n \, dt = H(\varepsilon_r) \qquad (47)$$

This in turn can be written as:

$$\sigma_m^n \; t_o \; K_{(n)} = H(\varepsilon_r) \qquad (48)$$

This expression provides another method for determining the value of n.

The material constant, n, can be determined using two test samples that have the same residual strain. The flow functions, which are single valued functions of strain at low work hardening levels, were equated for the two cases.

For small plastic strain values, the load time trace is identical to that for a fully hardened specimen loaded under the same conditions. This is illustrated in Figure 23. The form functions are, therefore, equal to those for a half sine pulse.

The expression for n that results from equating flow functions is given as:

$$n = \frac{\log\left(\frac{t_{o_2}}{t_{o_1}}\right)}{\log\left(\frac{\sigma_{m_1}}{\sigma_{m_2}}\right)} \qquad (49)$$

where σ_m refers to the peak stress and t_o is the pulse duration. The following values were used to determine n by this method:

$$\sigma_{m_1} = 41{,}724 \text{ p.s.i.} \quad t_{o_1} = 37.4 \text{ ms.} \quad \varepsilon_{r_1} = 0.28\%$$

$$\sigma_{m_2} = 39{,}250 \text{ p.s.i.} \quad t_{o_2} = 96.5 \text{ ms.} \quad \varepsilon_{r_2} = 0.27\%$$

The value of n was calculated as 15.5.

The strain rate values appearing in Figure *21* were assumed constant for each load pulse and were obtained from the slope of the linear portion of the trace in the pre-yield region. The decrease in slope at the onset of yielding, which appeared in some traces, was ignored. Another method exists to calculate n, that does not make any assumption regarding the pulse form.

The flow function at the yield point is the same for all specimens regardless of the load-time trace, as long as the initial dislocation density for each specimen is the same. It is assumed that detectable yielding occurs in all cases at the same small strain value and was preceded by micro-straining. The micro-strain can be described by the dynamic model equation expressed in equation *22*. Consequently, for the correct value of n, the value of the integral appearing in equation *47* should be the same for all load pulses. The integration is considered over the duration up to the yield point.

The relationship obtained in the above manner may be expressed as:

$$\int_{o}^{t_D} \sigma\,(t)^{\,n}\, dt \;=\; constant \qquad (50)$$

This equation is analogous to the one derived by Campbell[12] to describe the dynamic yielding of mild steel based on the Cottrell-Bilby dislocation release mechanism:

$$\int_{o}^{t_o} \left[\frac{\sigma\,(t)}{\sigma^{*}} \right]^{n} dt = \pi \qquad (51)$$

Where σ^{*} = the yield stress at 0^{o} K

π = the critical density of released dislocations necessary for yield to occur.

Several trial values of n were used to calculate the integral in equation *50*. Thirty-five load-time traces were used and for each value of n some scatter was observed in the results. This was expected due to the sensitivity of the integral for large values of n. For example, when n equals 20, a 1% error in the determination of the yield stress results in an 18.3% error in the value of the integral.

The coefficient of variance was used as a means to determine the best value of n. This coefficient is a measure of the dispersion of the results about the mean value. Figure *24* illustrates the variation of dispersion for different trial values of n. The minimum coefficient of variance or dispersion was found for a value of n equal to 13.2. Table *8* lists the values of the flow function for the best estimate of n.

4.3 Plastic Work

The second area of investigation, based on single impact results, concerned the linear relationship existing between the nominal

peak stress value and the residual strain. Tables *9* to *13* list the values of plastic strain that resulted from the nominal peak stresses indicated for each of the five time bases. The values in these tables are plotted in Figures *25* to *29* and illustrate the apparent linearity. The empirical constants for the straight line relationships of these figures are listed in Table *14*.

The large values of the correlation coefficients appearing in Table *14* indicate the degree of linearity existing between the elastic peak stress and strain. The y - intercept of the graphs in Figures *25* to *29* is called the apparent dynamic yield point. It is inferred by extrapolating the straight-line relationships that at this point, plastic flow is initiated. It is interesting to note that the apparent dynamic yield point decreases with an increase in pulse duration. This is to be expected, as the strain rate also decreases with increased pulse duration, due to the decrease in the slope of the rise portion of the trace. The slope of the straight line graphs also decreases with the time base increase.

An examination of the plastic strain energy yields an explanation for the experimentally observed linearity between elastic stress and plastic strain. If the intensifier is assumed to behave as a linear spring, then the energy it possesses upon being deflected is given as:

$$U = \frac{1}{2} \Gamma y^2 \qquad (52)$$

where Γ is the spring constant and y is the drive piston deflection. The energy involved in plastically deforming a specimen is equal to the difference between the energies possessed by the intensifier when deflected under elastic and plastic conditions. The plastic work is given as:

$$U_p = \frac{1}{2} \Gamma (y_e^2 - y_p^2) \tag{53}$$

where y_e and y_p are the maximum drive piston displacements for the two cases. The maximum drive piston displacement is derived as:

$$y = \frac{1}{A_3} \sqrt{\frac{2g \ H \ M \ V}{B}} \tag{54}$$

Referring to equation *31*, the maximum deflection can be expressed in terms of the maximum stress on the specimen:

$$y = \frac{A_1}{A_2 \ A_3} \cdot \frac{V}{B} \sigma \tag{55}$$

The spring constant can be expressed in terms of the intensifier parameters:

$$\Gamma = \frac{B \ A_3^2}{V} \tag{56}$$

The plastic work expression then becomes:

$$U_p = \frac{V}{2B} \left(\frac{A_1}{A_2}\right)^2 (\sigma_e^2 - \sigma_p^2) \tag{57}$$

The plastic work per unit volume, in terms of the residual strain, is given as:

$$U_p = \int_0^{\varepsilon_r} \sigma_p \, d \, \varepsilon_p \tag{58}$$

The idealized stress-strain curve for the specimen material is assumed to be elastic-linear strain hardening and the flow stress is expressed as:

$$\sigma_p = \sigma_{L.Y.} + q \, \varepsilon_p \tag{59}$$

The plastic work expression is therefore:

$$U_p = \sigma_{L.Y.} \, \varepsilon_r + q \, \frac{\varepsilon_r^2}{2} \tag{60}$$

and the plastic work for the total volume of the specimen is:

$$U_p = \left[\sigma_{L.Y.} \, \varepsilon_r + q \, \frac{\varepsilon_r^2}{2} \right] \cdot A_1 L_1 \tag{61}$$

where L_1 is the length of the specimen. Equating the two expressions for plastic work, and substituting the expression for σ_p given in equation 59, one obtains:

$$\sigma_e^2 = \frac{2B}{V} \left(\frac{A_2}{A_1} \right)^2 L_1 \left[\sigma_{L.Y.} \, \varepsilon_r + q \, \frac{\varepsilon_r^2}{2} \right] + \left[\sigma_{L.Y.} + q \, \varepsilon_r \right]^2 \tag{62}$$

where σ_e is the peak stress in the elastic load-time trace. A similar

analysis was performed by Harpolani[18] where the effects of work hardening were excluded.

Figures *26* and *27* illustrate the comparison between the theoretical elastic stress-plastic strain relationship and the experimental values for the 40 millisecond and 60 millisecond pulse durations. The value of q used in the above relation was 47.0×10^4 p.s.i. The dynamic lower yield point values for each time base, were obtained by taking an average value from the load-time traces. The lower yield point for the 40 milliseconds base was estimated to be 42,000 p.s.i. and for the 60 milliseconds base the estimated value was 39,000 p.s.i. The theoretical curves closely correspond to the experimental values and in the range of plastic strain considered, the relationship is approximately linear.

4.4 Flow Function

The dynamic loading of strain rate responsive material, permits higher stresses to be achieved prior to the initiation of plastic flow. Plastic flow also occurs in a finite period of time and as a result, for the same nominal peak load, greater residual strains result with longer pulse durations. For example, Tables *3* and *5* list two cases where the nominal peak stress was 71,000 p.s.i. The 14.6 millisecond pulse produced 1.03% strain, whereas the 64.1 millisecond pulse produced 4.1% strain.

Figure *30* illustrates the static peak stress-residual strain curve. Results for a typical dynamic test are also included in the figure. The dynamic curve was obtained by multiply impacting a specimen and recording the peak stress. The stresses for the dynamic curve are much larger than those for the static tests at the same strain level. The dynamic curve approaches the static curve as the strain and work hardening increase. The lower yield point in the static case appears to be in the area of 22,000 p.s.i. The shape of the dynamic curve was predicted by computer experiments using the mathematical model. The results will be discussed more extensively in Section 4.6 Table *15* lists the results of the static test that are plotted in Figure *30*.

Having obtained a value for n by the methods discussed in Section 4.2, the value of the flow functions for each impulse, could be determined. The results when plotted will provide an empirical curve relating dynamic load conditions to plastic deformation. The yield stress-strain rate method was considered to produce the most accurate value of n. This value was rounded to 20 for the purpose of flow function calculations. The maximum stress for a load pulse was calculated using the stress relation given in equation *34*.

The values of the flow function for single impact tests are listed in Table *16* along with the form functions and strain for each trace. Figure *31* is a log-log plot of the flow function. The theoretical curve also shown was obtained by piecemeal integration of

the dynamic model expression given in equation *23*. The experimental load-time traces were approximated by a triangular pulse of 10 milliseconds duration. The value of n was also 20. Other constants appearing in equation *24* were chosen so that the theoretical curve was similar to experimental values in magnitude and form. The values of the constants were in agreement with those for mild steel used by Hahn[3]. The values of the constants appearing in equation *24* were:

$$q = 43.54 \times 10^4 \text{ p.s.i.}$$

$$a = 1.0$$

$$C = 1.6 \times 10^9 \text{ cm/cm}^3 - \% \ \varepsilon_r$$

$$\sigma_o = 2.9 \times 10^4 \text{ p.s.i.}$$

$$b = 2.48 \times 10^{-8} \text{ cm.}$$

$$N_o^* = 10^3 \text{ cm/cm}^3$$

The function $H(\varepsilon_r)$ shown in Figure *31* is the value of the flow function when no-strain hardening occurs. At low values of strain $G(\varepsilon_r, t_o)$ approximates $H(\varepsilon_r)$.

4.5 Multiple Impacts

As stated in Section 3, the specimens were re-loaded several times at fixed intervals of time, under the same loading conditions, until no change was observed in the load-time traces or until buckling occurred in the specimens. The actual peak stress was observed to asymptotically approach the nominal peak stress value. Figures *32* and *33* show a typical series of load-time traces obtained by multiply impacting a specimen under constant load conditions. After seven

impacts it can be observed that the peak stress and pulse duration are identical to the corresponding values of the elastic test.

The plastic strain also approaches a limiting value. It is equal to the residual strain that would occur under static conditions when the specimen is loaded to the same stress as the nominal peak stress of the dynamic test. The static peak stress-residual strain results could not be used to attest to this fact because the maximum strains achieved were less than the limiting plastic strains reached during repeated dynamic loading.

Large plastic strains could not be achieved in static tests as buckling occurred. This did not occur in the dynamic tests until much larger strains were reached. The static test results appearing in Figure *30* were extrapolated to the region of strain achieved in the dynamic tests. The curve was approximated by a straight line and a linear strain hardening coefficient was estimated to be 47×10^4 p.s.i. This value is in close agreement with Hahn's[2] value of 43.5×10^4 p.s.i. The lower yield point was found by extending the curve to intersect the y-axis; the value was 22,000 p.s.i. The equation for the curve in Figure *30* is then given as:

$$\sigma = 22{,}000 + 47 \times 10^4 \ \varepsilon_r \text{ p.s.i.} \qquad (63)$$

Figure *34* illustrates the extension of the static peak stress-residual strain curve and a plot of the limiting dynamic strains against nominal peak stress. Thus, as long as buckling does not occur under dynamic load, the limiting strain is equal to the static value.

Multiple impacts under the same dynamic load conditions produced decreasing increments of plastic strain. The increments could be approximated by a geometric progression. The cumulative strain can therefore be represented as:

$$e_T = e_1 \cdot \frac{1 - r^m}{1 - r} \qquad (64)$$

where e_1 = residual strain after the first impact

m = number of impacts

and $r < 1$.

Figure *36* illustrates a typical comparison between the actual cumulative strain against impact number and the approximating geometric progression. In this example, the initial plastic strain was 2.8% and the fraction r was 0.8.

4.6 Flow Stress

Figure *36* indicates a typical drop in peak stress when a specimen was re-loaded in the low strain range. After the dynamic upper yield point is reached (Figure *37 a*), the mobile dislocation density in mild steel is increased at the rate of 2 to 4 x 10^9 cm/cm^3 per per cent plastic strain. This increase permits plastic flow to continue at a lower level of stress than the upper yield point (Figure *37 b*). Increased straining, however, requires a greater flow stress in order to overcome the effect of strain hardening.

A typical peak stress-residual strain curve derived from multiple impact tests is shown in Figure 30. The peak stress approaches the static test value required to produce the same residual strain.

The plastic flow model given in equation 22 can describe the significant peak stress drops that have been observed. The equation may be rearranged as:

$$\sigma = q\ \varepsilon_p + \sigma_o \left[\frac{\dot{\varepsilon}_p}{0.5b\ (N_o^* + C\ \varepsilon_p)} \right]^{1/n} \qquad (65)$$

If the effect of work hardening is neglected in the low strain region where peak stress drop occurs, the drop in stress from the upper dynamic yield can be expressed as:

$$\frac{\sigma_{U.Y.}}{\sigma_{L.Y.}} = \left[\frac{N_o^* + C\ \varepsilon_p}{N_o^*} \right]^{1/n} \qquad (66)$$

The above expression assumes that the plastic strain rate is constant over the stress drop range. Marsh and Campbell[11] obtained load time traces for mild steel that are similar to those obtained by the author. Figure 37 illustrates their results and indicates that the strain rate is constant over the stress-drop range.

A typical variation in peak stress drop with dislocation density for mild steel is illustrated in Figure 38. The increase in dislocation density, in the specimens tested, was brought about by pre-strain due to multiple impacts.

4.7 Cumulative Flow Function

The original design criterion, established by Kardos[4], predicted the residual strain in a material undergoing a single impulse of known amplitude and duration. No evidence existed regarding the validity of the expressions for the density and mobility of dislocations at relatively large plastic strain levels.

The empirical flow function derived from single impact tests and the cumulative flow function obtained from multiple impacts were described by the same curve. Thus, an equation of state was established that predicted the resultant strain from a load pulse, as long as the previous strain history was known.

The average number of impulses given to each specimen was fifteen. The flow function was determined from the oscilloscope trace for each impulse and the corresponding cumulative strain was measured. Figure *39* illustrates a log-log plot of the cumulative flow function against the cumulative residual strain for all specimens. The graph contains the results for each impulse. The results for all tests fall on a single curve. Thus, for a given plastic strain, the flow function is approximately a single value obtained from the data of a single pulse trace or from the summation of the flow functions of several pulses used to produce the same strain. The values plotted in Figure *31* also appear in Figure *39*.

The scatter of the experimental results about the theoretical curve is due primarily to the magnification of the error in calculating the maximum stress. The flow function depends on the value of this stress raised to the power n. Part of the reason for the dispersion is due to the difference in the time bases. Five time bases were used and for the same plastic strain, the flow function increases with increased pulse duration.

CHAPTER 5

DISCUSSION

5.1 Multiple Impact Model

The variation of the peak stress with increasing strain, as a result of multiple impacts, can be understood by examining the mathematical model derived in Chapter 2. Two factors effect the peak stress: the mobile dislocation density and the strain hardening. The degree of influence that each factor has on the resulting stress can be studied by artificially isolating each effect in the model equation.

If the integration is performed in equation *(23)*, the result is:

$$\int_0^{t_o} \left[\sigma(t) - q\,\varepsilon_p\right]^n dt = \frac{\sigma_o^n}{0.5bC} \log_e \left[1 + \frac{C}{N_o^*}\,\varepsilon_r\right] \qquad (67)$$

In the numerical experiments performed, a ramp load pulse was considered to be applied to the specimen. Yield was assumed to occur when a plastic strain of .1% was reached. The effect of strain hardening was neglected. The mobile dislocation density, N_o^*, was increased and the yield stress was then calculated. An expression for the equivalent strain is obtained from equation *9* as:

$$\varepsilon_{p_e} = \frac{N^* - N_o^*}{C} \qquad (68)$$

The model, therefore, assumes that straining brought about by multiple impacts causes an increase in the mobile dislocation density without producing a back stress due to hardening. Figure *40* illustrates the effect of dislocation density, on the yield stress. The density is expressed as an equivalent strain, using equation *68*. It can be deduced from Figure *40* that in the absence of strain hardening, an increase in dislocation density by straining brings about a continuous decrease in the flow stress.

The effect of work hardening can be studied by assuming that after each impulse a portion of the nucleated mobile dislocations is locked. The initial dislocation density prior to each loading is the same and the right hand side of equation *67* remains constant. The strain hardening term increases with each impulse. The yield stress for .1% incremental strain is determined. The net additional stress necessary to overcome strain hardening is the difference between the calculated yield stress and the yield stress for the same initial dislocation density without the hardening term. Figure *41* illustrates the effect of strain hardening for three different values of the linear strain hardening coefficient. A linear back stress-strain relationship exists. Combining the effects illustrated in Figures *40* and *41* produces a resultant stress-strain diagram. This is illustrated in Figure *42*.

Another study combined the strain hardening and density effects. Repeated ramp pulses were given to a specimen and the flow stress necessary to produce .1% incremental strain was calculated. This was

achieved by performing integration in steps in equation *67*. The results are plotted in Figure *43*. The form of a typical dynamic peak stress-residual strain curve obtained experimentally and shown in Figure *30* is similar to the theoretical curves in Figures *42* and *43*.

The cumulative effect of the flow function was also predicted using the dynamic model expressed in equation *67*. Table *17* lists a portion of the values used to plot the multiple impact curve seen in Figure *43*. The table shows the peak stress, cumulative strain and flow function for each of the first twelve load pulses on the specimen. After twelve impacts the cumulative plastic strain is given as 1.24% and the cumulative flow function is calculated as 1.67×10^{90}. Table *18* shows an excerpt from a table of values used to generate the theoretical flow function-residual strain curve seen in Figures *31* and *39*. These values were obtained for a triangular pulse of 10 milliseconds duration. The table indicates that for a single pulse with a peak stress of 47,000 p.s.i., the residual strain will be 1.22% and the flow function will be 1.32×10^{90}. These figures are within reasonable range of the plastic strain and cumulative flow function obtained by multiple impacts. The figures serve to illustrate that the final deformation can be determined for a series of impacts or a single impact as long as the empirical flow function-strain curve is known for the material. The effect of each pulse is additive in the flow functions.

5.2 Correlation

The dynamic behaviour of mild steel has been the object of a

great many experiments to date. Much of the results are presented in a form so as to relate delay times for yield as a function of the applied stress. In most cases the stress is constant with time. Carbon content, grain size and temperature have been observed as factors that influence the delay time for a given stress. A method has been discussed in Chapter 4.2 that uses the information of the log-log plot of yield stress against delay time to determine the dislocation velocity-stress exponent.

Table *19* lists the values of n obtained for mild steel by this author and values derived from the log-log plots of delay time against stress, provided by other authors. The results from other sources were, for the most part, based on constant stress application and approximately the same temperature of 73^{0} F. at which the present experiments were performed. The values for n found by methods discussed in this paper coincide with results of other tests.

The actual delay times in the tests performed by the author are considerably larger than for the other experiments. Equation *23* can be employed to express the relation between delay times for constant stress application and for constant stress rate application, the latter mode of loading being used in the experiments described herein. The delay times for constant stress rate are $(n + 1)$ times those for constant stress pulses, the peak stress being identical.

A complete comparison of the values listed in Table *19* could not be made as the heat treatment for some of the specimens was not available.

It would appear that the value of n for mild steel lies in the range of 10 to 25. The precise value depends on the particular carbon content and heat treatment for the material.

The dislocation velocity-stress exponent n is an important material characteristic and knowledge of its order of magnitude permits some insight into the dynamic behaviour of a polycrystalline material. Materials having small values of n have pronounced yield drops and long delay times before the onset of macroscopic yielding. Also, small values of n are associated with strain rate responsive materials. An observable change in the upper dynamic yield stress occurs with a substantial change in the applied strain rate. The value of n varies greatly for different materials and mild steel is in the lower region. Values as low as 5 have been recorded for single crystals of chromium[10] and Armco iron[17] and values as high as 300 in the case of silver[3].

The dynamic model can be used to describe another phenomenon of yield-delay time experiments. It has been observed that when a constant stress pulse is applied for a period less than the delay time for that stress level, yielding will occur on re-loading in a time equal to the difference between the delay time and the period of the previous pulse.

It has been stated that the flow function in the low strain region is solely dependent on residual strain and it equals the product $\sigma_m^n \, t_o \, K(n)$. If a specimen is loaded repeatedly before macroscopic yielding occurs, then the yield point can be predicted by determining

the flow functions for each load pulse. Yielding will occur when the sum of the flow functions for each pulse equals the yield point flow function $H(\varepsilon_y)$, where ε_y, is the residual strain at yield.

For constant stress application the ratio of the flow function for a pulse duration, t, to that for yielding is t/t_y. If a specimen is re-loaded after this pulse duration, the yield-delay time is reduced to $(1 - t/t_y) \cdot t_y$ assuming that the stress level is the same for both pulses. Clark[15] refers to tests on mild steel in which the load is removed when 3/5 of the delay time had elapsed. The samples showed no apparent yield. On subsequent re-loading the delay time was found to be 2/5 of that for a single pulse producing yield.

5.3 Recommendations

The experimental apparatus provided a suitable means of examining some aspects of the dynamic behaviour of materials. For future studies with the present equipment, the following recommendations are suggested.

1. Other strain rate responsive materials should be examined and the value of n determined. This would have a two fold purpose. The validity of application of the dynamic model to other materials could be derived to provide a design reference for dynamic loading of that material.

2. The effect of variation of carbon content and grain size in mild steel could be examined.

3. The intensifier volume and drop tester height ranges could be extended to provide a wider variance in strain rate.

4. Observation of dynamic effects would be facilitated if the load time traces for multiple impacts were superimposed on the same photograph. This would require precise triggering of the oscilloscope trace. It is suggested that a photocell replace the microswitch as the triggering mechanism.

5. The effect of time interval between load pulses should be examined, and the results compared with those of this paper. The material should also be heat treated between loads to examine this effect on the peak stress.

6. A strain-time record should be made on all tests. For this reason, it is suggested that an extensometer be fixed to the drive piston of the intensifier.

7. It is suggested that a Hopkinson bar might be added to the present dynamic test equipment. This, together with a static compressive tester, would permit a continuous variation of strain rate from approximately 10^{-3} sec^{-1} to 10^{6} sec^{-1}.

CONCLUSION

The form of the flow function curve can be described by a dynamic model that is based on the microdynamical theory of plasticity. Appropriate material constants for mild steel were substituted into the model and a theoretical curve was derived to fit the experimental data. The results were illustrated in Figure *31*.

The cumulative flow function curve was plotted from the multiple impact test data. The results could be described by the same curve used to fit the single impact data. As a result, the flow function-strain relationship can be considered as an equation of state. The plastic strain, resulting from a dynamic load pulse, can be predicted as long as the strain history of the specimen is known.

In multiple impact tests where buckling did not occur ultimately the actual peak stress and total plastic strain both approached limiting values. The peak stress value attained after repeated impacts approximated the nominal peak stress for the dynamic load series. The resultant cumulative strain approached the value that would have been obtained in a static test for a stress level equal to the nominal peak stress.

The variation of cumulative strain with impact number can be described by a geometric progression. The constants for the expression

are dependent upon the nominal peak stress and pulse duration of the semi-sinusoidal load pulse.

The dynamic peak stress-residual strain curves were compared to the static test results. The upper dynamic yield point varied with strain rate in the approximate range of 44,000 p.s.i. to 55,000 p.s.i. The upper dynamic yield was considered to be the point at which a sudden drop occurred in the load-time trace, prior to reaching the nominal peak stress.

The lower yield point in static tests was approximately 22,000 p.s.i. A direct comparison could not be made between the upper dynamic yield points of the static and dynamic tests as the static value was not obtained. However, it can be inferred from Figure *38*, which illustrates the yield drop in mild steel, that a drop in excess of 35% is unlikely. This would indicate an upper static yield of approximately 30,000 p.s.i.

A theoretical stress-strain curve was derived for dynamic loading using the mathematical model. The form of the peak stress-strain curve for multiple impact tests was similar to the theoretical curve. In tests where the initial plastic strain was small, the peak stress was observed to decrease on re-loading under the same conditions. After repeated loading the peak stress that the specimen could support, before further yielding, increased in a manner similar to the theoretical curve.

In conclusion, the initial, intermediate and limiting values of plastic strain can be predicted for a series of repeated dynamic loads

of known magnitude, form and duration.

REFERENCES

1. *Johnston, W.G. and Gilman, J.J.*

   "Dislocation Velocities, Dislocation Densities, and Plastic Flow in Lithium-Fluoride Crystals"
   Journal of Applied Physics, Volume 30, No.2. February 1959.

2. *Hahn, G.T.*

   "A Model for Yielding with Special Reference to the Yield-Point Phenomena of Iron and Related BCC Metals"
   Acta Metallurgica, Volume 10, August 1962.

3. *Hahn, G.T., Reid, C.N. and Gilbert, A.*

   "Dislocation Dynamics of Yielding and Fracture"
   U.S. Air Force System Command Technical Documentary Report No. ASD-TDR-63-324.

4. *Kardos, G.*

   "A Study of Plastic Flow in Steel at High Rates of Strain"
   Ph.D. Thesis, Mechanical Engineering, McGill University, July 1965.

5. *Gilman, J.J. and Johnston, W.G.*

   "Behaviour of Individual Dislocations in Strain-Hardened Li F Crystals"
   Journal of Applied Physics, Volume 31, No. 4. April 1960.

6. *Gilbert, A., Wilcox, B.A. and Hahn, G.T.*

   "The Effect of Strain Rate on Dislocation Multiplication in Polycrystalline Molybdenum"
   Philosophical Magazine, 11, 649, (1965).

7. *Reid, C.N.*

   "Dislocation Multiplication"
   Philosophical Magazine, Volume 11, 409, (1965).

REFERENCES (CONTINUED)

8. *Keh, A.S. and Weissmann, S.*

"Electron Microscopy and Strength of Crystals"
Interscience: New York 1963.

9. *Hahn, G.T. and Gilbert, A.*

"Further Investigation of Notch Sensitivity of Refractory Metals"
U.S. Air Force System Command Technical Documentary Report No. ASD-TDR-62-1004.

10. *Reid, C.N., Gilbert, A. and Hahn, G.T.*

"Dislocation and Deformation Modes in Chromium Single crystals"
Transactions of the Metallurgical Society of A.I.M.E., Volume 239, April 1967 - 467.

11. *Marsh, K.J. and Campbell, J.D.*

"The Effect of Strain Rate on the Post-Yield Flow of Mild Steel"
Journal of the Mechanics and Physics of Solids, 1963, Volume 11.

12. *Campbell, J.D.*

"The Dynamic Yielding of Mild Steel"
Acta Metallurgica, Volume 1, November 1953.

13. *Hendrickson, J.A. and Wood, D.A.*

"The Effect of Rate of Stress Application and Temperature on the Upper Yield Stress of Annealed Mild Steel"
Transactions of the American Society of Metals, Volume 50, 1958.

14. *Kraft, J.M. and Sullivan, A.M.*

"Effect of Grain Size and Carbon Content on the Yield Delay-Time of Mild Steel"
Transactions of the American Society of Metals, Volume 51, 1959.

REFERENCES (CONTINUED)

15. *Kardos, G.*

"Response of Metals to High Strain Rates - A Review of the Literature"
Space Research Institute of McGill University, Report No. 64-1.

16. *Clark, D.S.*

"The Behaviour of Metals Under Dynamic Loading"
Transactions of the American Society of Metals, Volume 46, 1954.

17. *Sinha, S.K.*

"Plastic Strain in Materials Under the Influence of Impulsive Load"
Master's Thesis, Mechanical Engineering Department, McMaster University, May 1968.

18. *Harpolani, K.*

"The Dynamic Yielding of Mild Steel"
Master's Thesis, Mechanical Engineering Department, McMaster University, May 1969.

19. *Gilman, J.J.*

"Microdynamical Theory of Plasticity"
Microplasticity - Advances in Materials Research, Volume 2, Interscience Publishers 1968.

20. *Gilman, J.J.*

"Physical Nature of Plastic Flow and Fracture"
Plasticity - Proceedings of the Second Symposium on Naval Structural Mechanics, Pergamon Press - 1960.

21. *Mendelson, Alexander*

"Plasticity : Theory and Application"
The Macmillan Company, 1968.

22. *Abbe, E.H.*

"Determination of Yield Strengths of Engineering Materials at High Loading Rates"
Proceedings on the Dynamic Behaviour of Materials and Structures, U.S. Army Conference 1962.

REFERENCES (CONTINUED)

23. *Cottrell, A.H.*

"Discontinuous Yielding"
The Relation Between the Structure and Mechanical Properties of Metals, Volume II, National Physical Laboratory Conference 1963.

24. *Campbell, J.D. and Duby, J.*

"Delay Yield and Other Dynamic Loading Phenomena in a Medium - Carbon Steel"
Proceedings of the Conference on the Properties of Materials at High Rates of Strain, 1957
The Institution of Mechanical Engineers.

25. *Kolsky, H.*

"The Propagation of Mechanical Pulses in Anelastic Solids"
Colloquium on the Behaviour of Materials Under Dynamic Loading, American Society of Mechanical Engineers 1965.

26. *Campbell, J.D.*

"An Investigation of the Plastic Behaviour of Metal Rods Subjected to Longitudinal Impact"
Journal of the Mechanics and Physics of Solids, 1953, Volume I.

27. *Gilman, J.J.*

"Dynamical Behaviour of Dislocations"
Symposium on the Mechanical Behaviour of Materials Under Dynamic Loads, Army Research Office, Durham 1967.

28. *Hull, D. and Noble, F.*

"Indirect Measurements of the Effect of Stress on the Velocity of Dislocations"
Dislocations in Solids, Faraday Society, 1964.

29. *Johnston, W.G.*

"Yield Points and Delay Times in Single Crystals"
Journal of Applied Physics, Volume 33, No. 9
September 1962

TABLE 1

INTENSIFIER VARIABLES

DROP WEIGHT LB.	VOLUME $IN.^3$	PISTON AREA $IN.^2$	PULSE DURATION MS.
36.25	3.11	.8824	14.6
47.50	34.96	.8824	36.6
139.00	120.34	.8824	64.1
139.00	120.34	.3725	175.9
252.00	120.34	.3725	246.2

TABLE 2

PEAK FORCE - DROP HEIGHT CONSTANTS

$P.F.\ (lbs.) = D \times H\ (in.)^{p}$

PULSE DURATION	D	p	CORRELATION
14 ms.	4,002	0.57	0.989
40 ms.	1,767	0.65	0.977
60 ms.	5,490	0.49	0.999
170 ms.	7,587	0.44	0.998
240 ms.	13,920	0.36	0.994

TABLE 3

SINGLE IMPACT DATA - 14 MILLISECONDS

ELASTIC TEST			PLASTIC TEST			
STRESS RATE $\frac{P.S.I.}{SEC.} \times 10^{-7}$	PEAK STRESS $P.S.I. \times 10^{-3}$	PULSE TIME MS.	YIELD STRESS $P.S.I. \times 10^{-3}$	YIELD TIME MS.	PULSE TIME MS.	STRAIN %
1.10	58.68	15.20	48.56	4.47	16.08	0.63
1.30	71.03	14.88	48.60	3.79	17.18	1.02
1.31	71.71	15.00	48.13	3.71	16.97	1.03
1.46	69.81	14.99	53.90	3.94	17.66	1.19
1.50	73.36	14.36	53.08	3.67	16.72	1.27
1.61	80.43	15.15	51.84	3.30	18.47	1.59
1.98	103.39	13.93	51.65	2.38	18.59	2.58
2.16	109.60	14.20	50.93	2.64	19.55	2.87
2.77	116.54	14.73	54.52	2.09	20.52	3.68
2.73	133.31	14.21	55.62	1.86	20.76	4.38

TABLE 4

SINGLE IMPACT DATA - 40 MILLISECONDS

ELASTIC TEST			PLASTIC TEST			
STRESS RATE $\frac{P.S.I.}{SEC.} \times 10^{-7}$	PEAK STRESS $P.S.I. \times 10^{-3}$	PULSE TIME MS.	YIELD STRESS $P.S.I. \times 10^{-3}$	YIELD TIME MS.	PULSE TIME MS.	STRAIN %
0.127	46.78	38.66	44.08	14.88	41.00	0.71
0.275	50.20	37.84	47.38	13.76	40.14	1.05
0.299	56.48	35.94	48.12	13.01	42.88	1.51
0.328	62.80	36.73	50.16	11.88	44.93	2.30
0.241	69.02	36.57	50.47	11.80	45.08	3.13
0.487	76.29	34.35	52.09	10.13	43.45	3.67

TABLE 5

SINGLE IMPACT DATA - 60 MILLISECONDS

ELASTIC TEST			PLASTIC TEST			
STRESS RATE $\frac{P.S.I.}{SEC.} \times 10^{-7}$	PEAK STRESS $P.S.I. \times 10^{-3}$	PULSE TIME MS.	YIELD STRESS $P.S.I. \times 10^{-3}$	YIELD TIME MS.	PULSE TIME MS.	STRAIN %
0.146	41.93	67.1	41.86	28.9	70.25	0.52
0.148	46.61	66.5	46.09	27.9	67.49	0.97
0.217	53.69	63.5	46.64	21.3	70.25	2.13
0.265	60.72	63.4	48.49	20.7	72.20	3.19
0.160	66.71	62.4	49.00	19.5	71.93	3.68
0.228	71.45	62.0	50.07	17.4	71.10	4.17

TABLE 6

SINGLE IMPACT DATA - 170 MILLISECONDS

ELASTIC TEST			PLASTIC TEST			
STRESS RATE $\frac{P.S.I.\times10^{-7}}{SEC.}$	PEAK STRESS P.S.I.x10^{-3}	PULSE TIME MS.	YIELD STRESS P.S.I.x10^{-3}	YIELD TIME MS.	PULSE TIME MS.	STRAIN %
0.063	48.53	197.45	44.05	70.67	226.62	1.91
0.079	57.78	181.46	45.27	54.12	235.87	3.14
0.094	64.95	173.48	44.91	45.53	225.16	3.90
0.107	70.83	167.35	44.84	45.33	222.97	4.74
0.132	81.36	160.09	47.32	38.59	213.36	5.82

TABLE 7

SINGLE IMPACT DATA - 240 MILLISECONDS

ELASTIC TEST			PLASTIC TEST			
STRESS RATE $\frac{P.S.I.}{SEC.} \times 10^{-7}$	PEAK STRESS $P.S.I. \times 10^{-3}$	PULSE TIME MS.	YIELD STRESS $P.S.I. \times 10^{-3}$	YIELD TIME MS.	PULSE TIME MS.	STRAIN %
0.072	83.19	261.00	46.01	59.26	346.54	6.94
0.083	91.49	250.48	45.75	51.44	337.75	7.64
0.079	87.65	254.72	45.93	53.89	352.73	7.71
0.096	101.18	238.61	45.08	45.25	341.05	9.86
0.106	105.77	232.55	46.19	40.38	339.01	10.5
0.117	113.74	228.09	45.84	36.15	329.40	12.0

TABLE 8

YIELD POINT FLOW FUNCTIONS

n = 13.2

$H(\epsilon r) \times 10^{-59}$

0.46
0.47
0.58
0.63
0.81
0.81
0.82
0.82
1.04
1.14
1.29
1.43
1.54
1.55
1.57
1.58
1.75
2.05
2.11
2.16
2.63
2.88
2.89
2.91
2.97
2.97
3.02
3.08
3.21
3.37
3.41
3.95
4.22
4.74
5.77

Coefficient of Dispersion = 0.5917

TABLE 9

NOMINAL PEAK STRESS VS. STRAIN - 14 MILLISECONDS

DROP HEIGHT IN.	NOMINAL PEAK STRESS P.S.I. x 10^{-3}	STRAIN %
6.375	58.68	0.63
7.875	71.30	1.03
8.375	69.81	1.19
11.375	80.43	1.59
14.825	103.39	2.58
16.375	109.60	2.87
21.375	116.54	3.68
24.375	133.31	4.38

TABLE 10

NOMINAL PEAK STRESS VS. STRAIN - 40 MILLISECONDS

DROP HEIGHT IN.	NOMINAL PEAK STRESS P.S.I. x 10^{-3}	STRAIN %
11.5625	46.78	0.71
12.8225	50.20	1.05
14.0625	56.48	1.51
16.0625	69.02	3.13
17.0625	62.80	2.30
23.0625	76.29	3.67

TABLE 11

NOMINAL PEAK STRESS VS. STRAIN - 60 MILLISECONDS

DROP HEIGHT IN.	NOMINAL PEAK STRESS P.S.I. x 10^{-3}	STRAIN %
2.4375	41.93	0.52
2.9375	46.61	0.97
3.9375	53.69	2.13
4.9375	60.72	3.19
5.9375	66.71	3.68
6.9375	71.45	4.17

TABLE 12

NOMINAL PEAK STRESS VS. STRAIN - 170 MILLISECONDS

DROP HEIGHT IN.	NOMINAL PEAK STRESS P.S.I. x 10^{-3}	STRAIN %
1.8125	48.53	1.91
2.8125	57.78	3.14
3.8125	64.95	3.90
4.8125	70.83	4.74
6.3125	81.36	5.82

TABLE 13

NOMINAL PEAK STRESS VS. STRAIN - 240 MILLISECONDS

DROP HEIGHT IN.	NOMINAL PEAK STRESS P.S.I. x 10^{-3}	STRAIN %
1.8125	83.19	6.94
2.8125	91.49	7.64
3.8125	101.18	9.86
4.3125	105.77	10.50
5.3125	113.74	12.04

TABLE 14

NOMINAL PEAK STRESS - RESIDUAL STRAIN CONSTANTS

$$N.P.S.\ (P.S.I.) = S\ (P.S.I.) \times \epsilon_r + c\ (P.S.I.)$$

PULSE DURATION	S	c	
MS.	P.S.I. x 10^{-6}	P.S.I. x 10^{-3}	CORRELATION
14.6	1.928	49.85	0.992
36.6	1.002	39.32	0.995
64.1	0.771	38.00	0.996
175.9	0.835	32.11	0.998
246.2	0.526	41.90	0.925

TABLE 15

STATIC TEST DATA

STRESS P.S.I.	ϵ_1^* %	ϵ_2^* %
17,500	0.12	0.08
20,000	0.15	0.10
22,500	0.21	0.27
25,000	0.90	0.96
27,500	2.07	1.71
30,000	2.30	2.05
32,500	2.57	2.58
35,000	2.94	2.84
37,500	3.44	3.32
40,000	4.05	3.92
42,500	4.62	4.84
45,000	5.50	5.60

* Subscripts refer to the two samples tested.

TABLE 16

SINGLE IMPACT FLOW FUNCTIONS

PULSE DURATION MS.	NOMINAL PEAK STRESS P.S.I.x10^{-3}	FORM FUNCTION	FLOW FN. x 10^{-89}	STRAIN %
16.08	58.68	0.109	0.439	0.63
17.18	71.03	0.146	0.715	1.02
16.97	71.71	0.154	0.609	1.03
17.66	69.81	0.057	1.612	1.19
16.72	73.36	0.057	1.120	1.22
18.47	80.43	0.083	1.252	1.59
18.59	103.39	0.291	3.834	2.58
19.55	109.60	0.157	1.939	2.87
20.53	116.54	0.091	3.311	3.68
20.76	133.31	0.079	6.244	4.38
41.00	46.78	0.127	0.202	0.71
40.14	50.20	0.114	0.818	1.02
42.88	56.48	0.121	0.915	1.51
44.93	62.80	0.102	1.857	2.30
45.08	69.02	0.103	2.141	3.13
43.45	76.29	0.088	3.140	3.67

TABLE 16 (CONT'D)

PULSE DURATION MS.	NOMINAL PEAK STRESS P.S.I.x10^{-3}	FORM FUNCTION	FLOW FN. x 10^{-89}	STRAIN %
70.25	41.93	0.152	0.159	0.52
67.49	46.61	0.116	0.839	0.97
70.25	53.69	0.119	0.036	2.13
72.20	60.72	0.122	1.823	3.19
71.93	66.71	0.151	3.730	3.68
71.10	71.45	0.182	6.275	4.17
226.62	48.53	0.071	0.570	1.91
235.87	57.78	0.094	1.177	3.14
225.16	64.95	0.173	1.918	3.90
222.97	70.83	0.190	1.033	4.74
213.36	81.36	0.185	76.612	5.82
346.54	83.19	0.196	206.105	6.94
337.75	91.49	0.175	385.627	7.64
352.73	87.65	0.185	478.359	7.71
341.05	101.18	0.194	3,181.750	9.86
339.01	105.77	0.186	6,671.732	10.50
329.40	113.74	0.196	30,379.470	12.04

TABLE 17

MULTIPLE IMPACT MODEL

PEAK STRESS P.S.I. x 10^{-3}	STRAIN %	FLOW. FN. - G (ϵ_r, t_o) x 10^{-90}
42.30	0.10	0.6775
38.40	0.20	0.0888
37.90	0.30	0.0675
37.80	0.41	0.0638
37.80	0.51	0.0638
37.90	0.62	0.0675
38.10	0.72	0.0753
38.30	0.83	0.0841
38.50	0.93	0.0940
38.80	1.03	0.1102
39.10	1.14	0.1298
39.40	1.24	0.1522

$G(\epsilon_r, t_o) = 1.6745 \times 10^{90}$

TABLE 18

FLOW FUNCTION DATA - DYNAMIC MODEL

PEAK STRESS P.S.I. x 10^{-3}	STRAIN %	FLOW FUNCTION x 10^{-90}
40.0	.00005	0.05
41.0	.00010	0.08
42.0	.00023	0.13
43.0	.00068	0.22
44.0	.00300	0.35
45.0	.02788	0.55
46.0	.37221	0.85
47.0	1.22913	1.31

TABLE 19

DISLOCATION VELOCITY PARAMETERS

n	CARBON CONTENT	METHOD	REFERENCE
25.00	0.12%	Yield-Delay Time (Const. Stress)	Vreeland, Wood & Clark[12]
18.07	0.14%	Yield-Delay Time (Const. Strain Rate)	Burke
15.00	0.17%	Yield-Delay Time (Const. Stress)	Hendrickson & Wood[13]
13.00	0.17%	Yield-Delay Time (Const. Stress)	Kraft - Sullivan[14]
14.10 19.30	0.17% 0.19%	Yield-Delay Time (Const. Stress)	Clark[16]
19.68	0.14%	Stress-Strain Rate	Burke
11.00	-	Stress-Strain Rate	Manjoine[15]
18.80	0.2 %	Yield-Delay Time (Const. Strain Rate)	Morrison[12]
15.50	0.14%	Stress-Time (Equal Form Fns.)	Burke
13.20	0.14%	Equal Yield Flow Functions	Burke

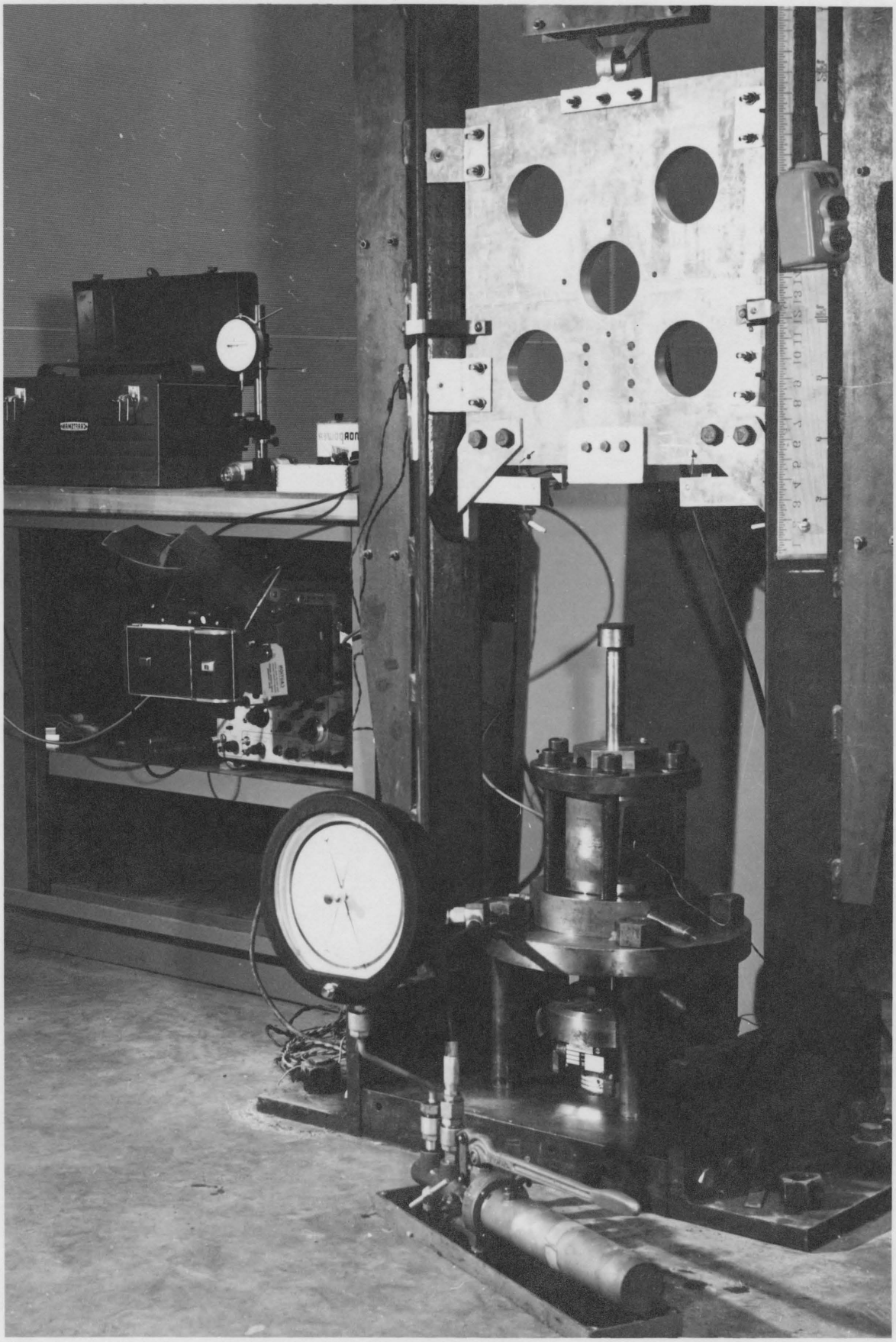

FIGURE 1

EXPERIMENTAL

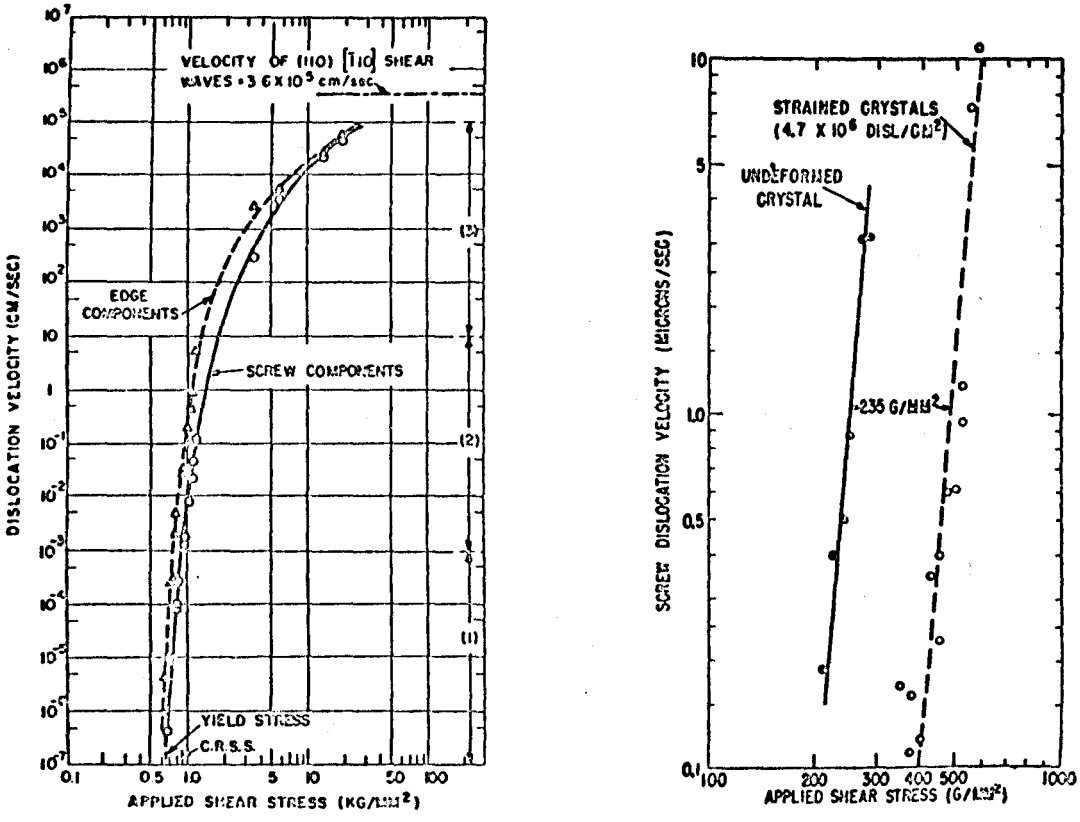

2a 2b

FIGURE 2*. a. Variation of dislocation velocity with applied shear stress in LiF crystals

b. Effect of strain on dislocation mobility in LiF

* See Reference 3

FIGURE 3*

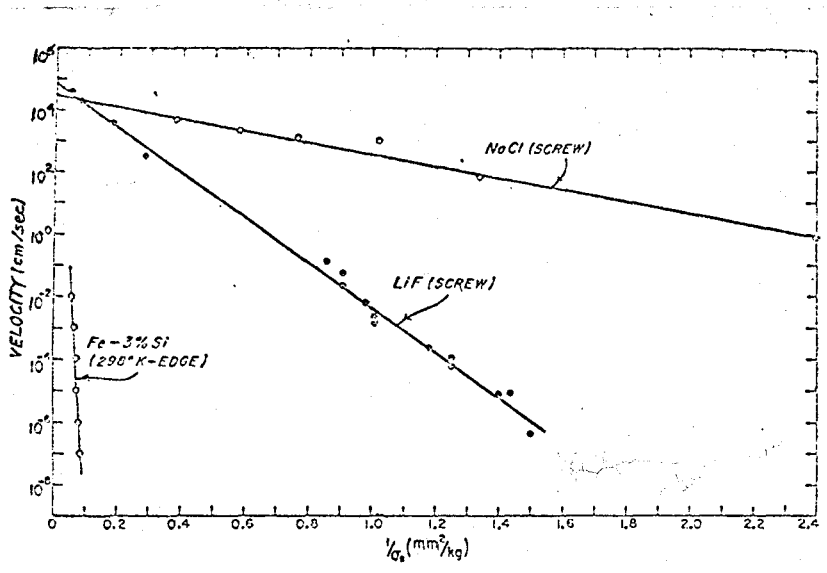

LOG DISLOCATION VELOCITY VS.

RECIPROCAL OF STRESS

* See Reference 19

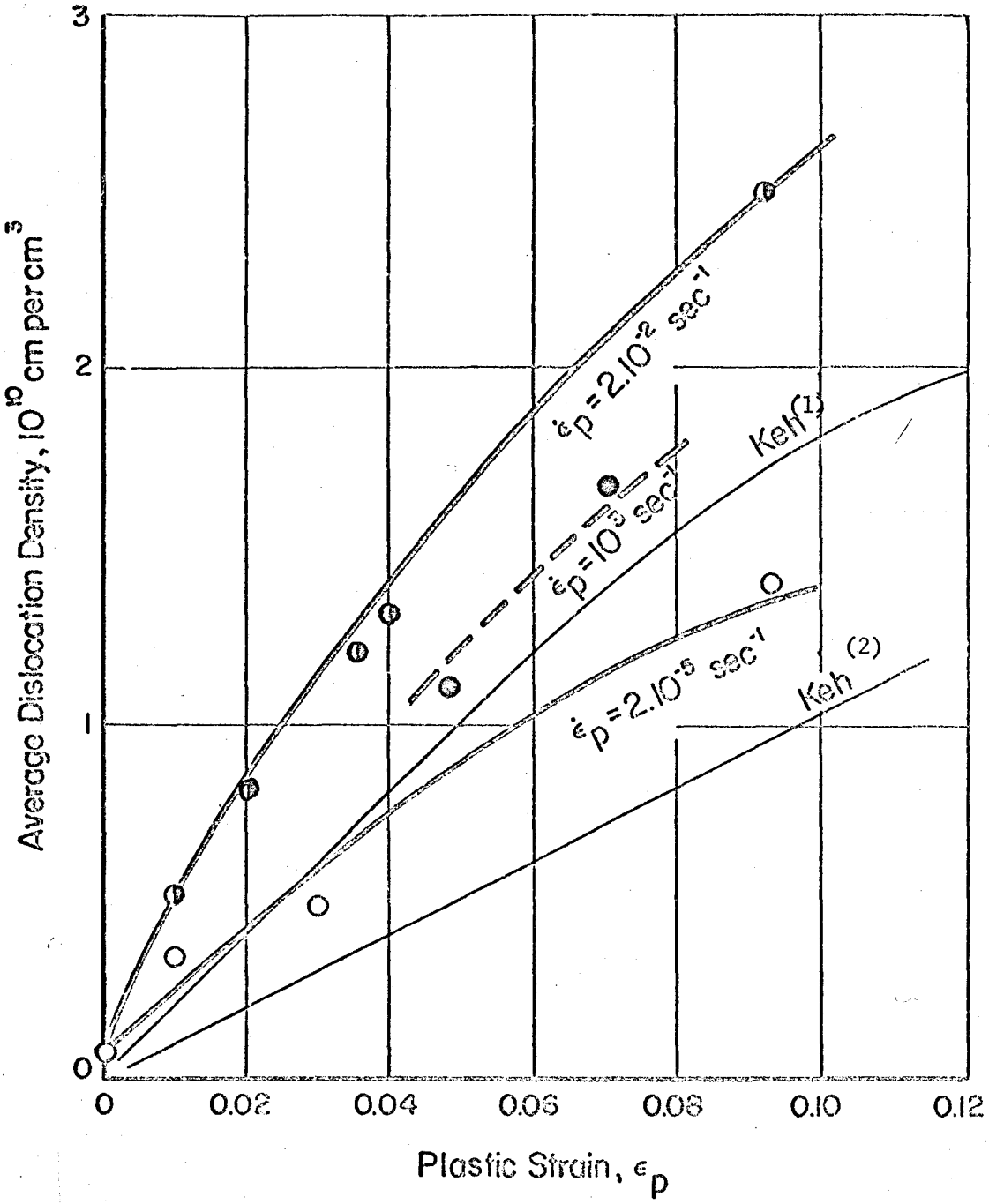

○ ◑ ● Mild Steel, C-0.25, Mn-1.00 G.S. ~ 0.02 mm (Hahn[3])
Keh[8] (Iron) $\dot{\epsilon}_p = 2.10^{-4}$
(1) G.S. ~ 0.015 mm
(2) G.S. ~ 0.10 mm

FIGURE 4.* INCREASE OF DISLOCATION DENSITY WITH STRAIN IN MILD STEEL DEFORMED AT DIFFERENT RATES.

* See Reference 3

FIGURE 5 *

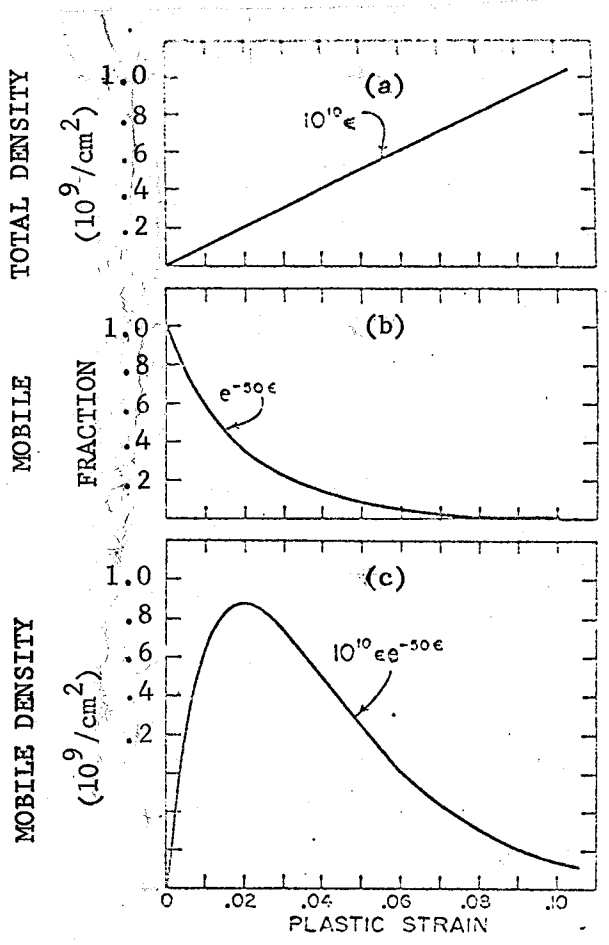

GRAPHICAL EXAMPLES OF THE CHANGES

WITH INCREASING PLASTIC STRAIN OF:

a) TOTAL DISLOCATION DENSITY

b) MOBILE FRACTION OF DISLOCATIONS

c) MOBILE DISLOCATION DENSITY

* See Reference 19

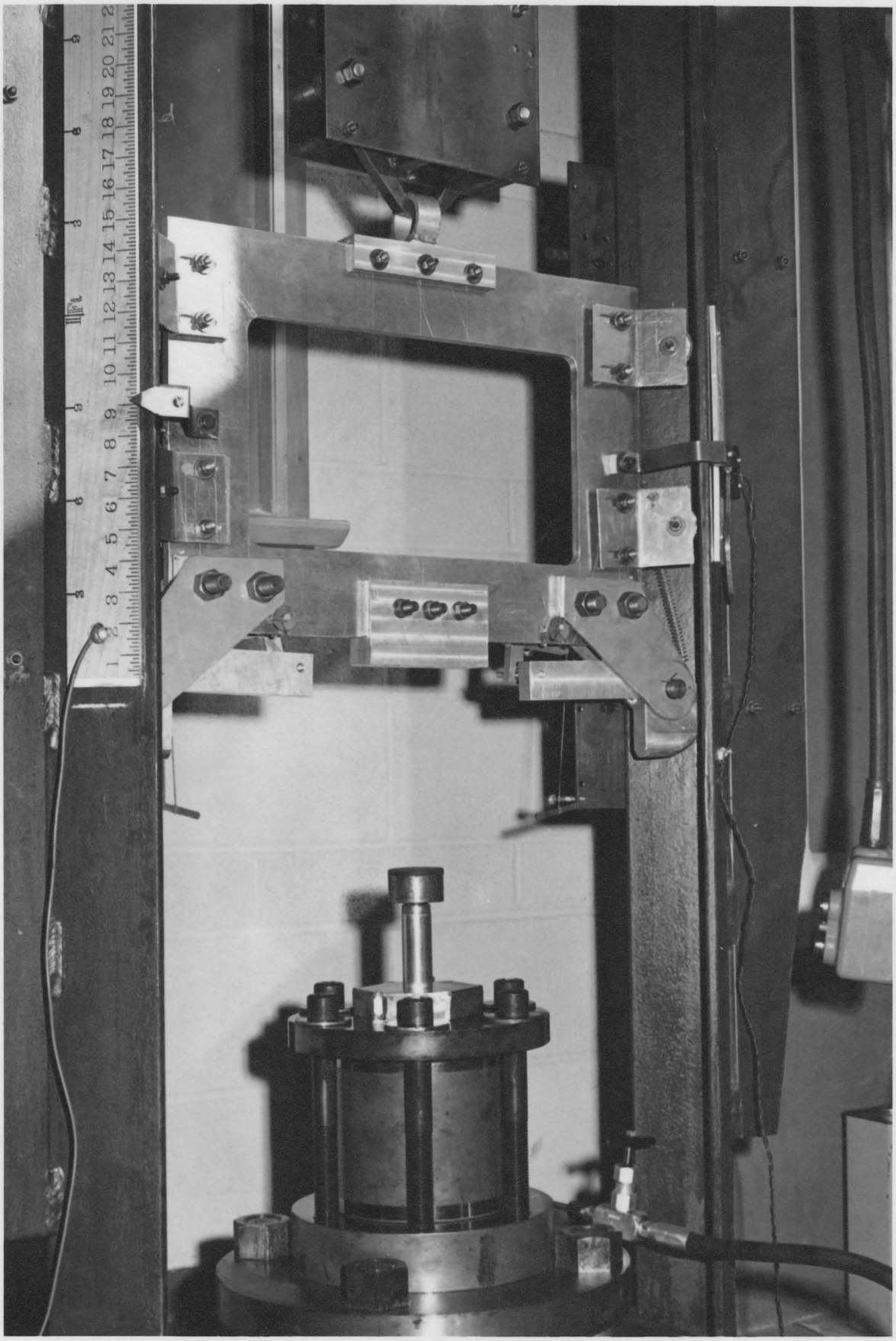

HYDRAULIC INTENSIFIER AND DROP TABLE

FIGURE 7

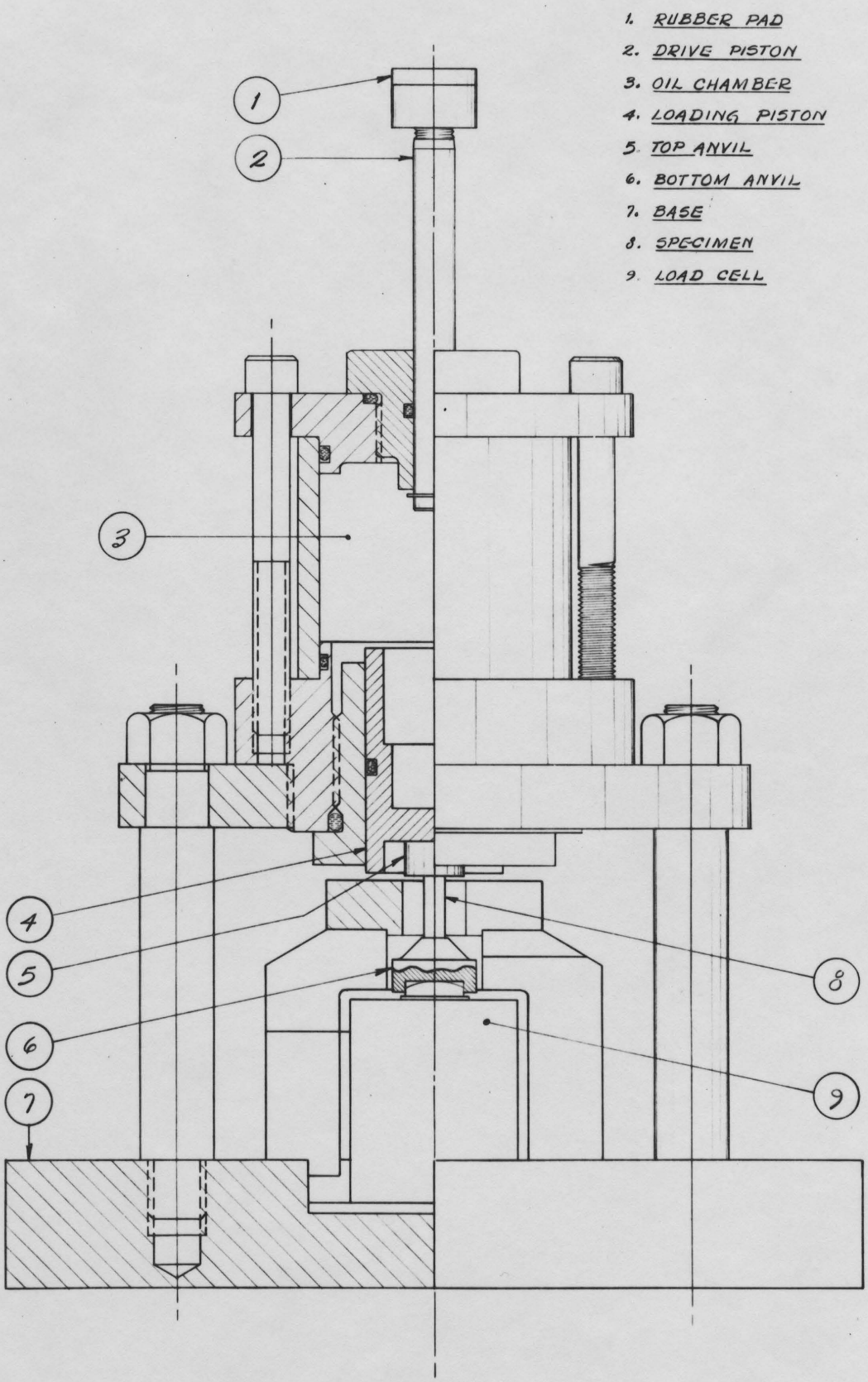

SECTIONAL VIEW OF THE HYDRAULIC INTENSIFIER

FIGURE 8

A TYPICAL ELASTIC RESPONSE

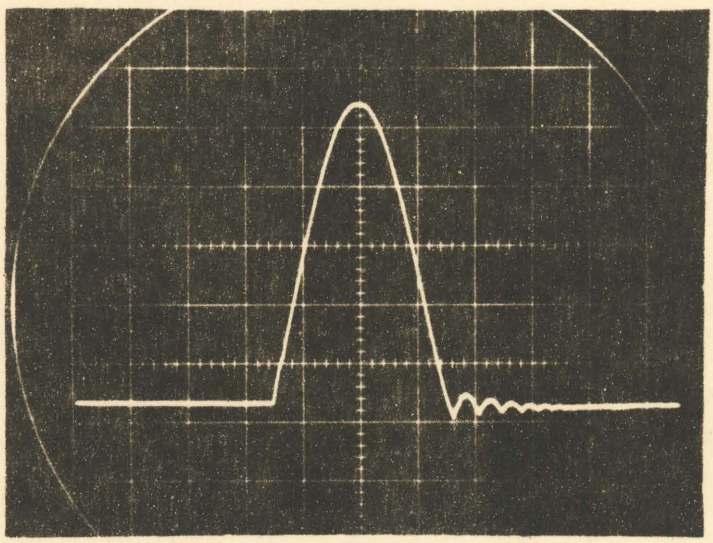

FIGURE 9 - 14 MILLISECONDS

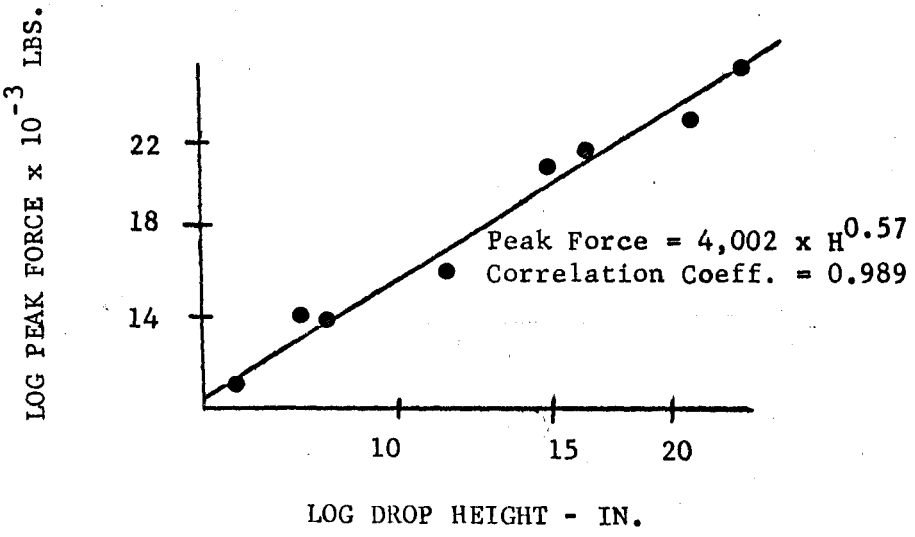

FIGURE 10 - 40 MILLISECONDS

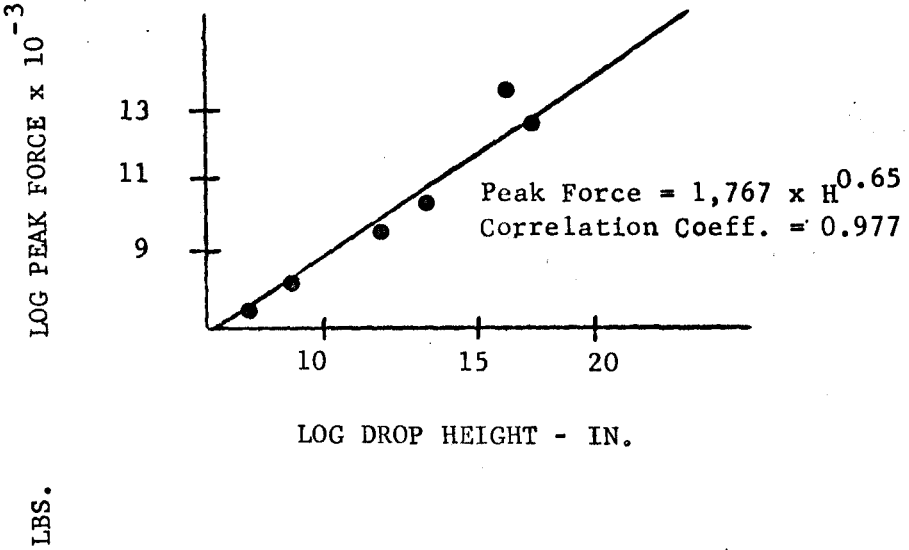

FIGURE 11 - 60 MILLISECONDS

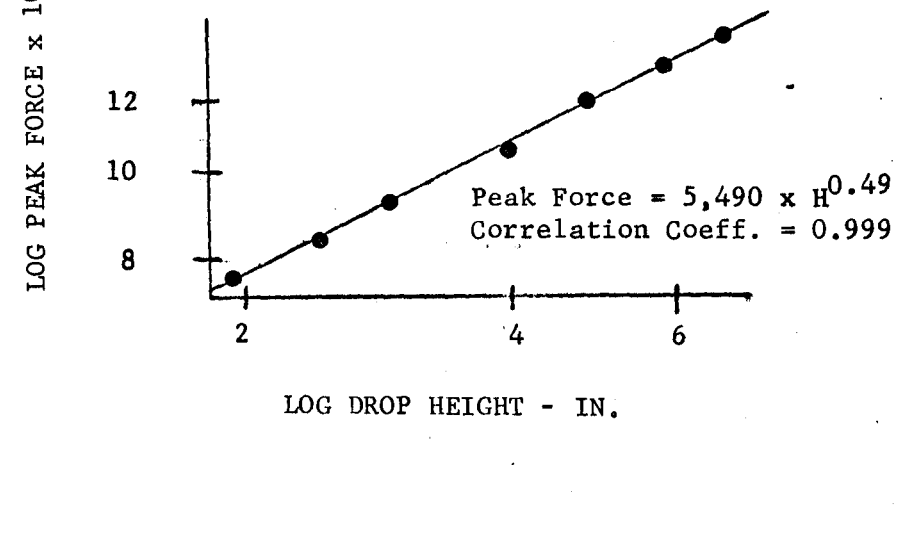

FIGURE 12 - 170 MILLISECONDS

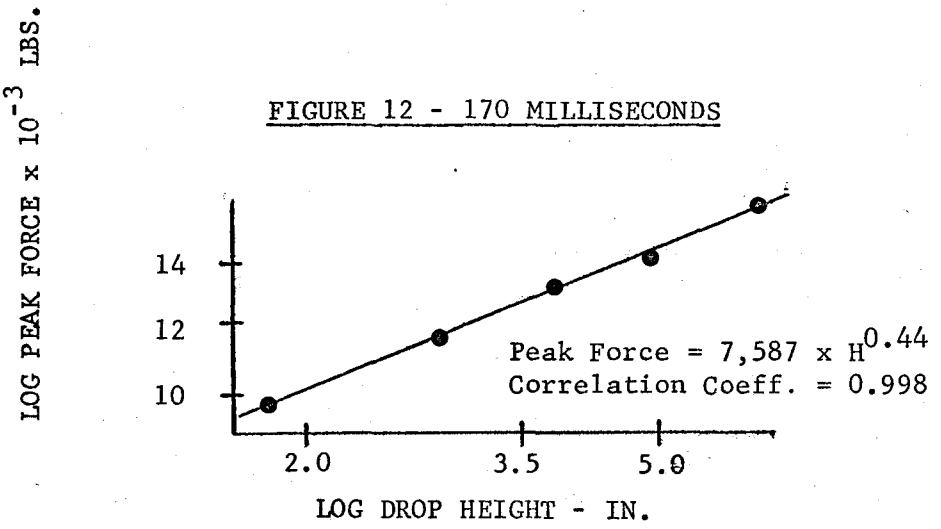

FIGURE 13 - 240 MILLISECONDS

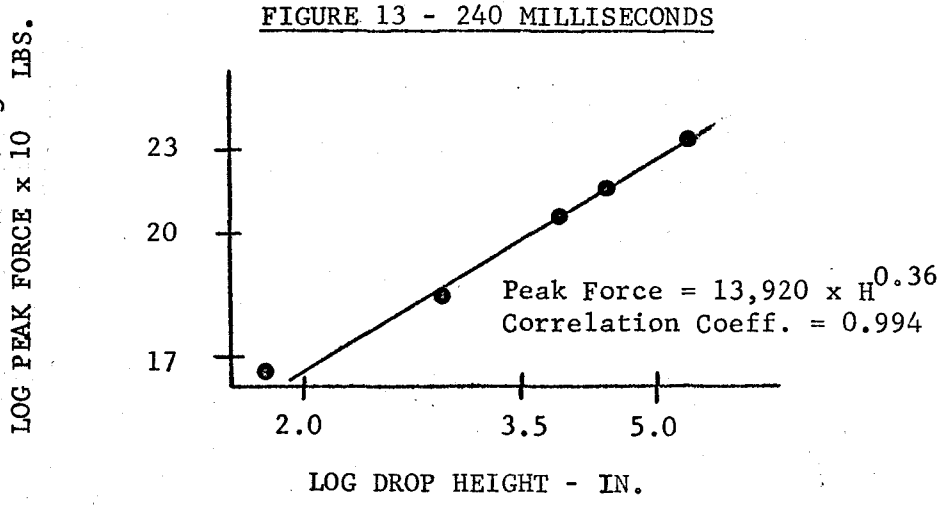

FIGURE 14

TYPICAL LOAD TIME TRACES

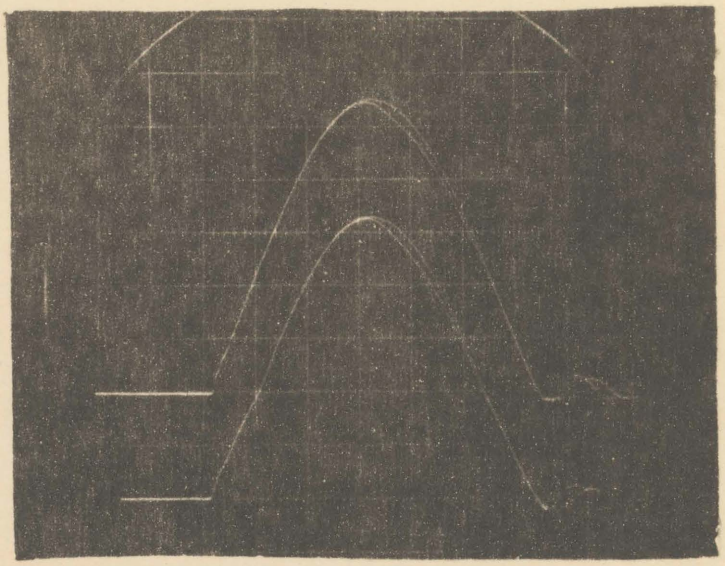

FIGURE 14 a SMALL STRAIN

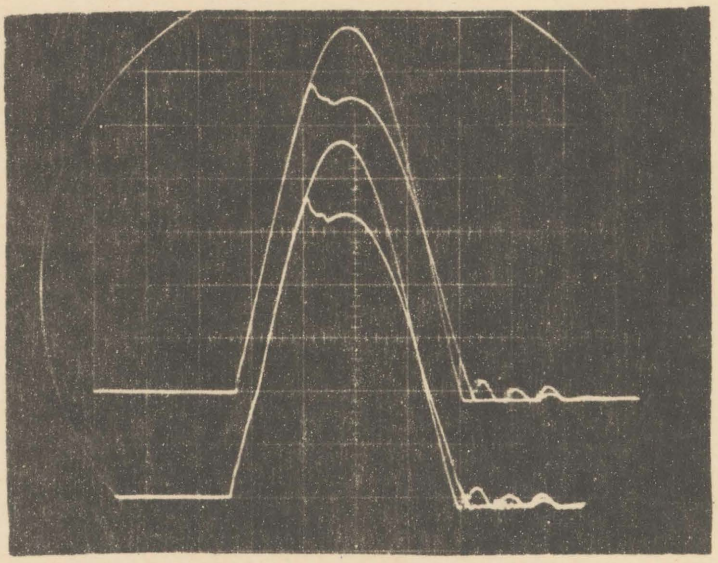

FIGURE 14 b LARGE STRAIN

FIGURE 15

LOAD TIME TRACES - 14 MILLISECONDS

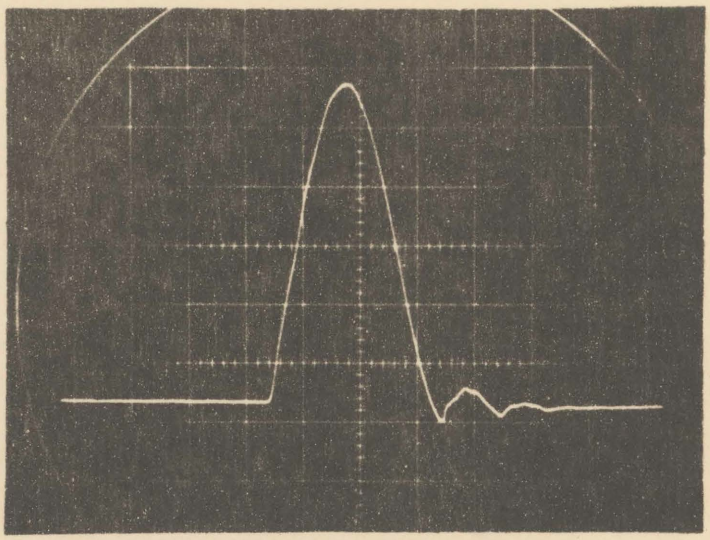

FIGURE 15 a ELASTIC RESPONSE

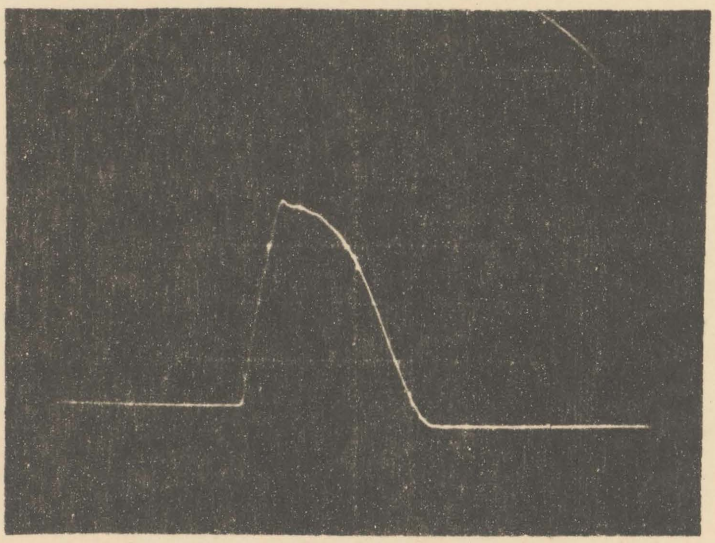

FIGURE 15 b PLASTIC RESPONSE

FIGURE 16

LOAD TIME TRACES - 40 MILLISECONDS

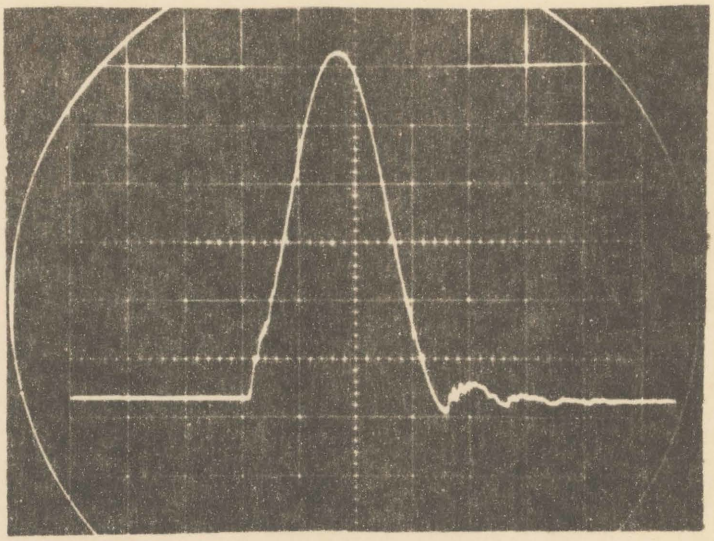

FIGURE 16 a ELASTIC RESPONSE

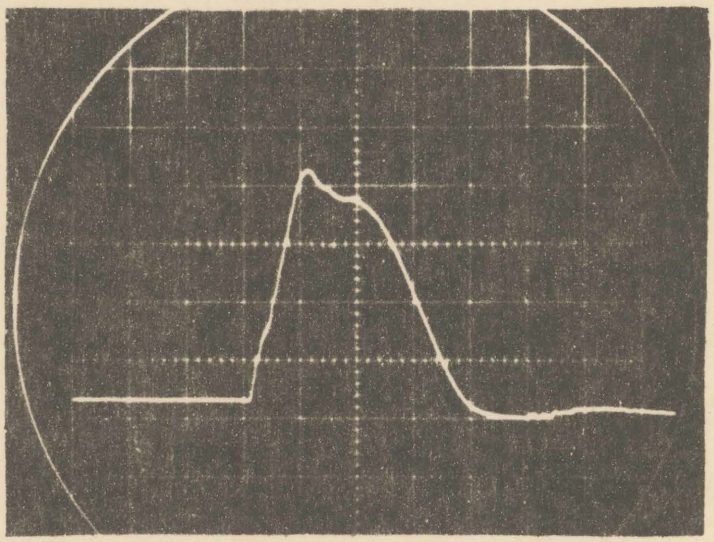

FIGURE 16 b PLASTIC RESPONSE

FIGURE 17

LOAD TIME TRACES - 60 MILLISECONDS

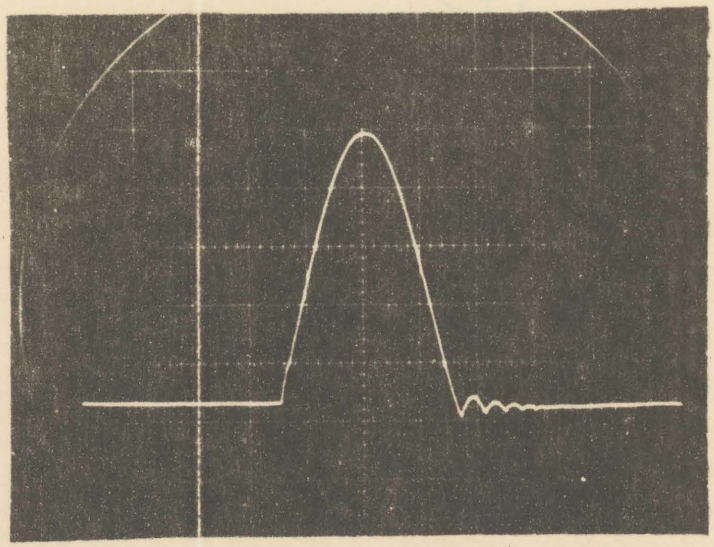

FIGURE 17 a ELASTIC RESPONSE

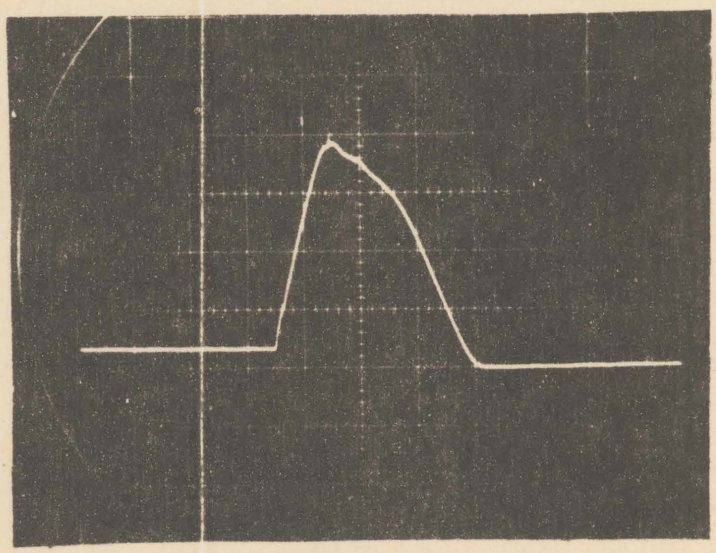

FIGURE 17 b PLASTIC RESPONSE

FIGURE 18

LOAD TIME TRACES - 170 MILLISECONDS

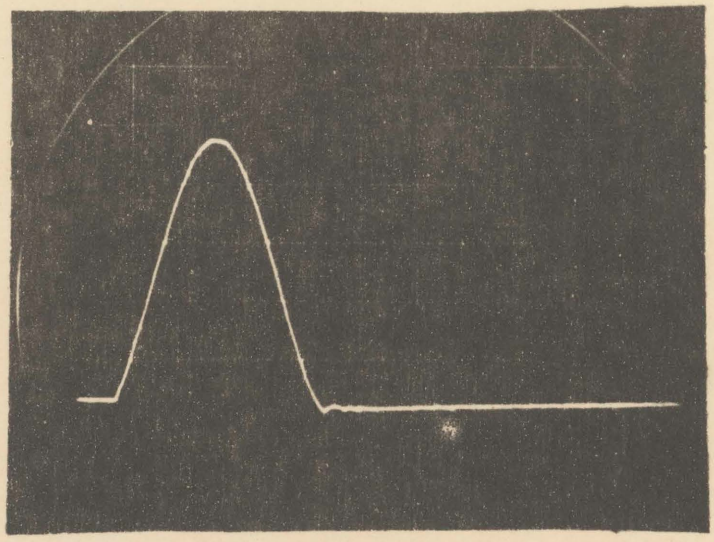

FIGURE 18 a ELASTIC RESPONSE

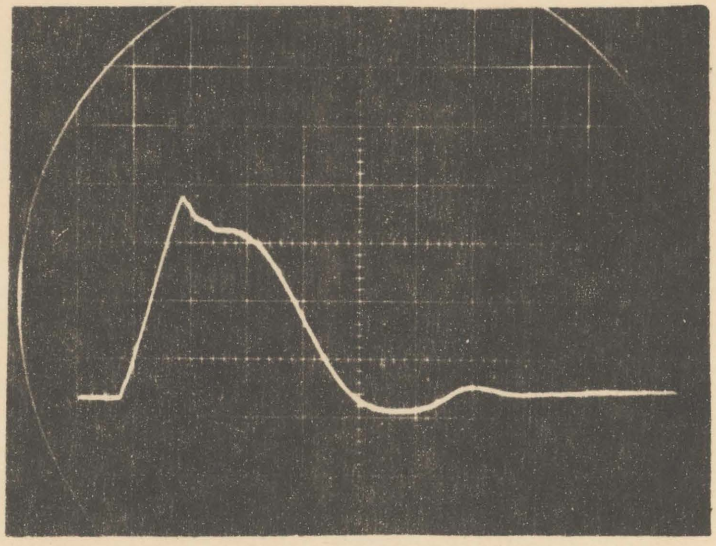

FIGURE 18 b PLASTIC RESPONSE

FIGURE 19

LOAD TIME TRACES - 240 MILLISECONDS

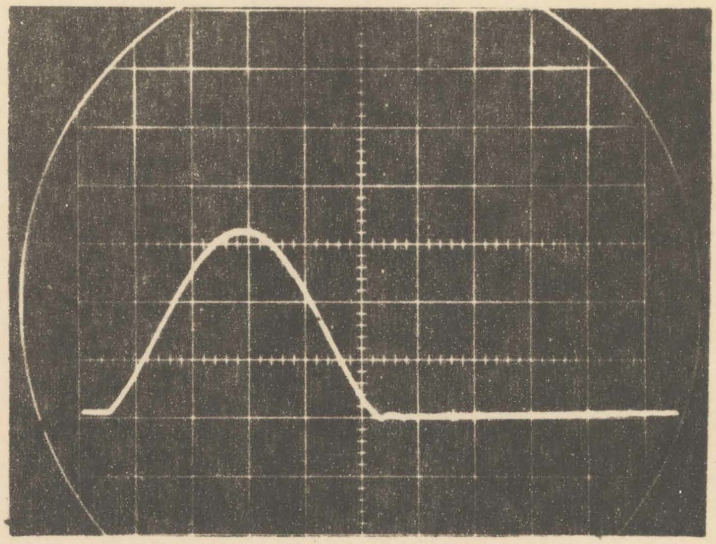

FIGURE 19 a ELASTIC RESPONSE

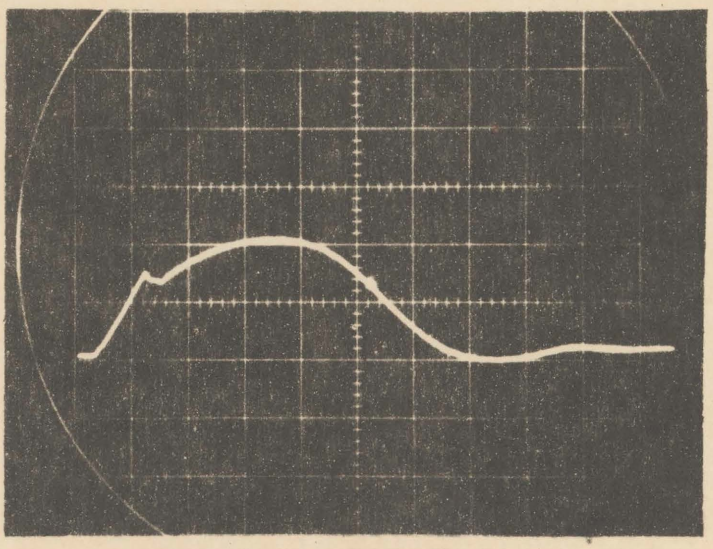

FIGURE 19 b PLASTIC RESPONSE

FIGURE 20

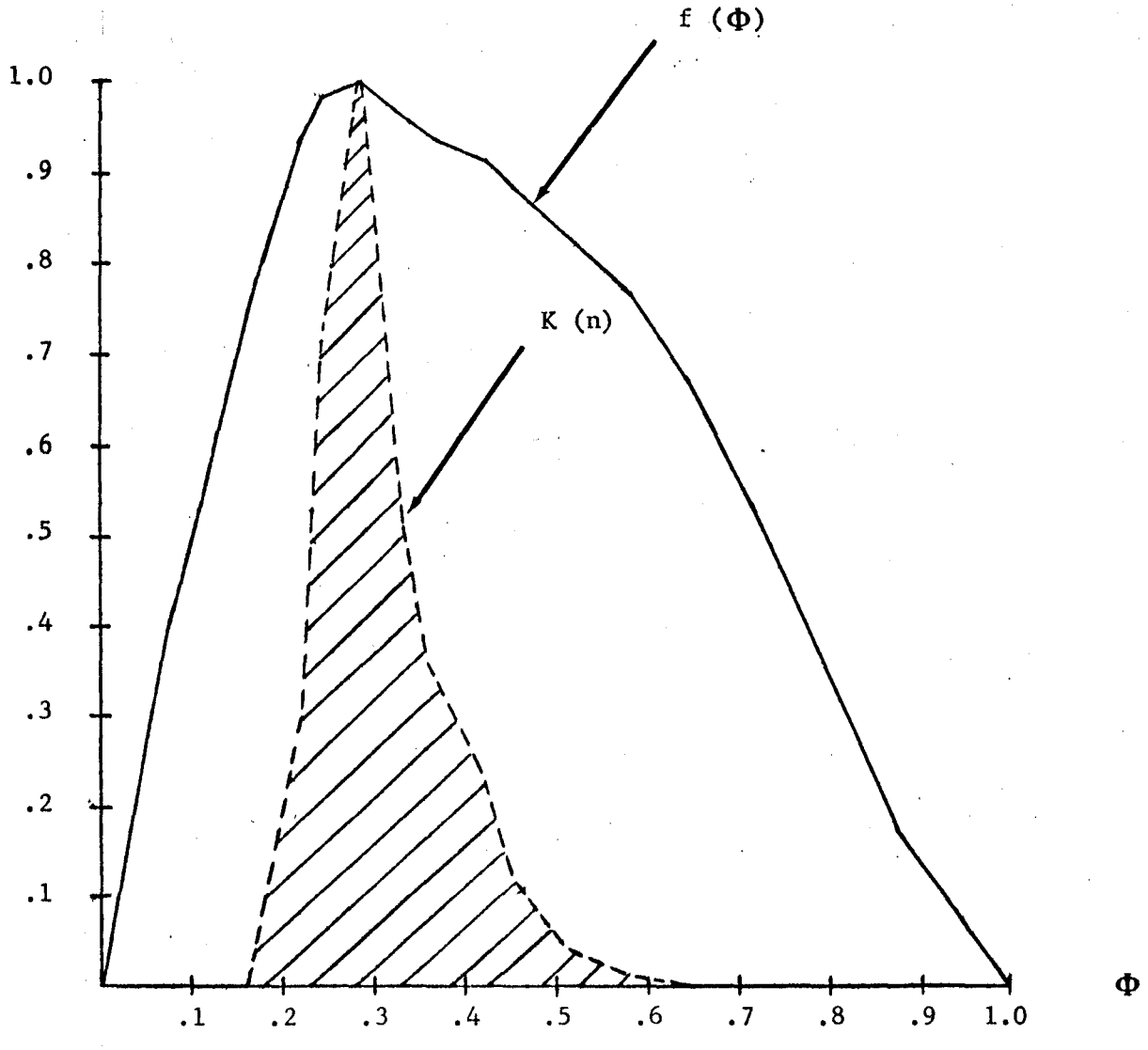

NON-DIMENSIONAL LOAD-TIME TRACE AND FORM FUNCTION

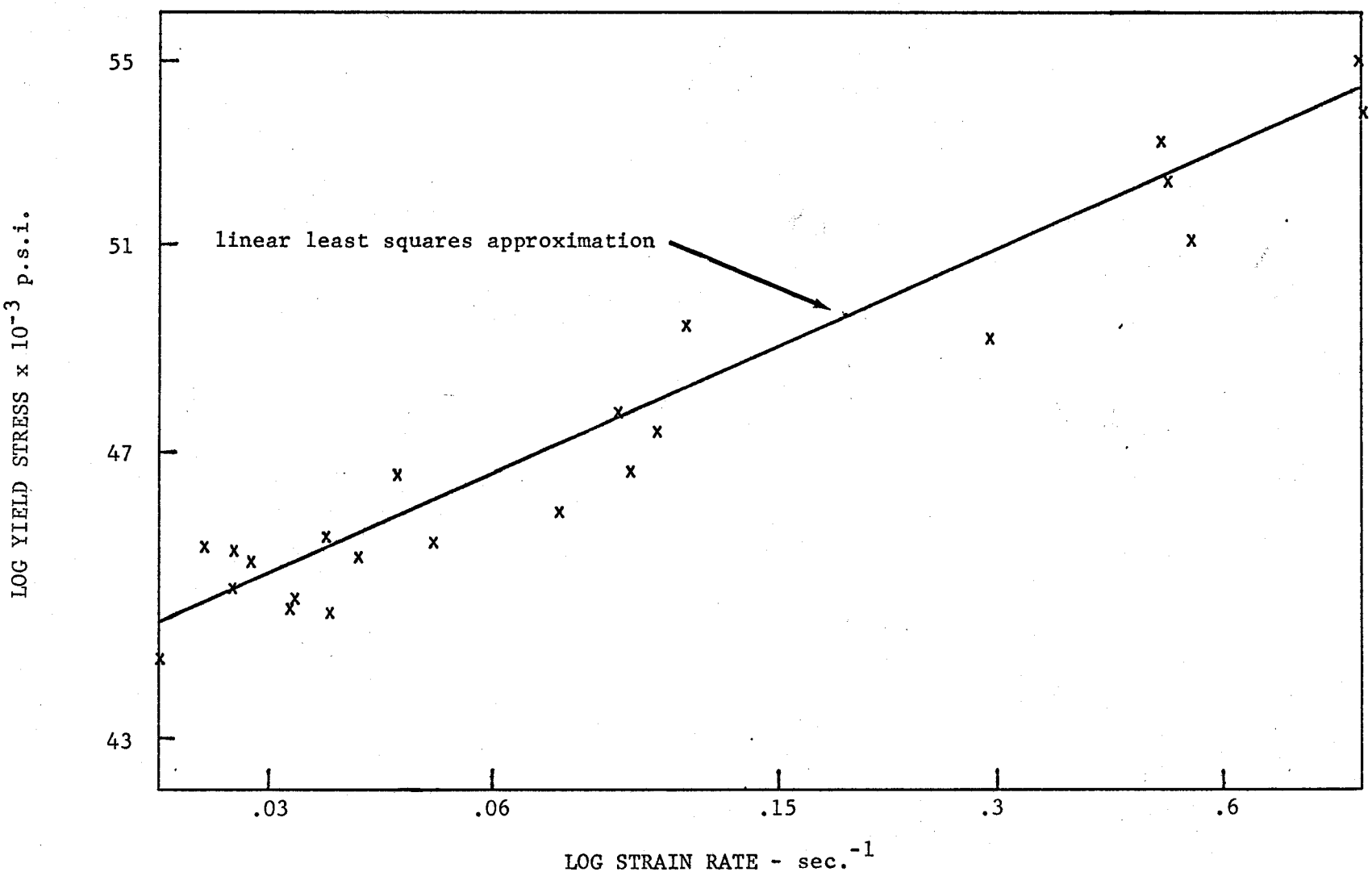

FIGURE 21 YIELD STRESS VS. STRAIN RATE

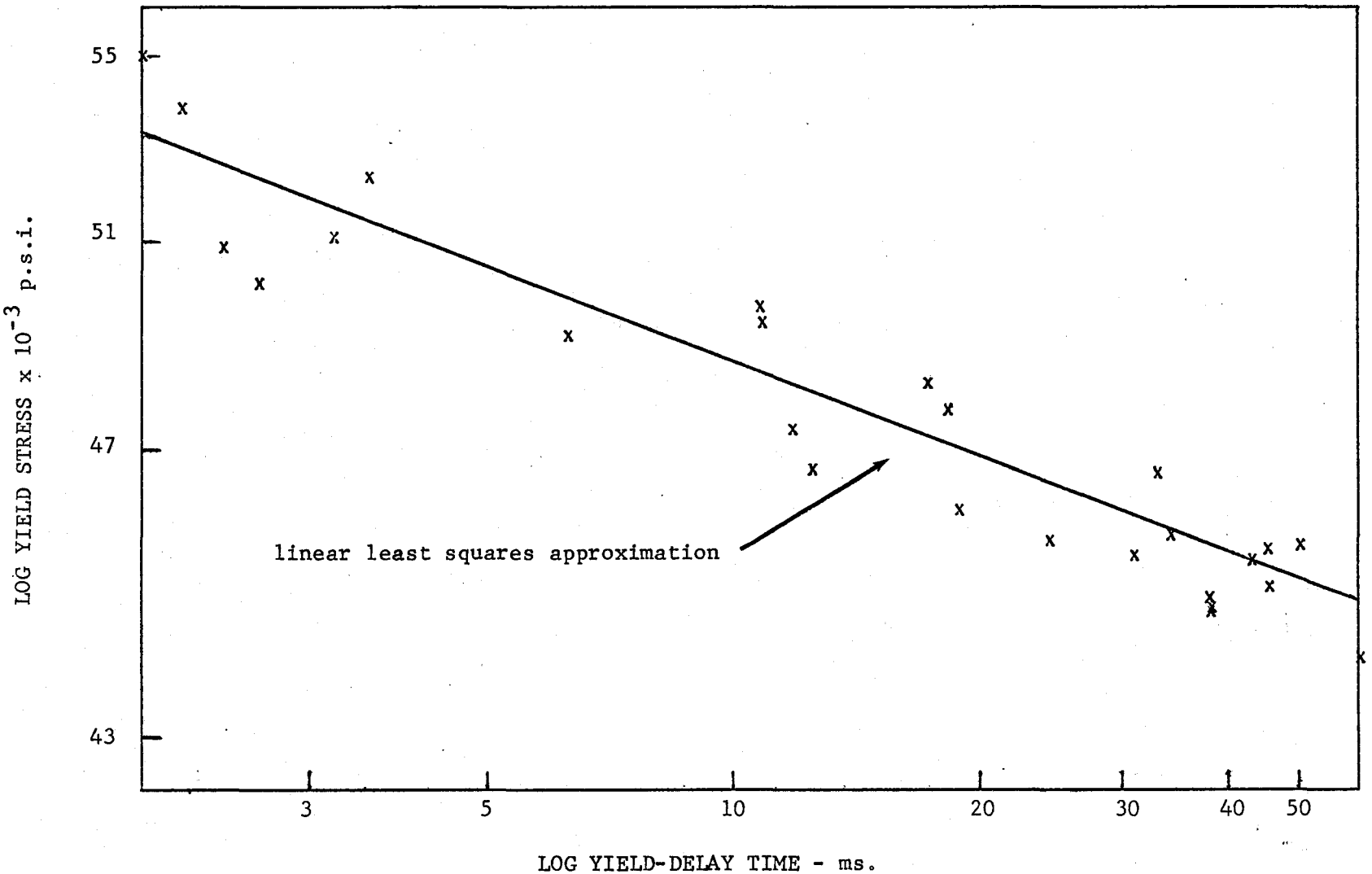

FIGURE 22 YIELD STRESS VS. DELAY TIME

FIGURE 23

LOAD-TRACES (SMALL RESIDUAL STRAIN)

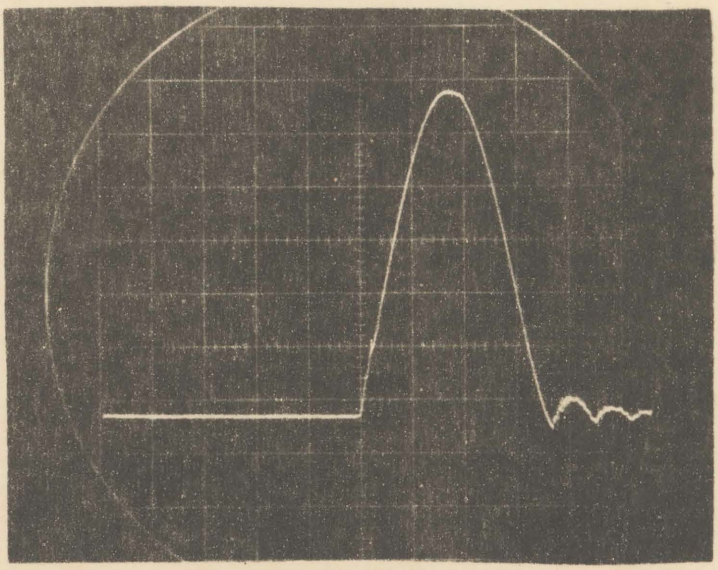

FIGURE 23 a ELASTIC RESPONSE

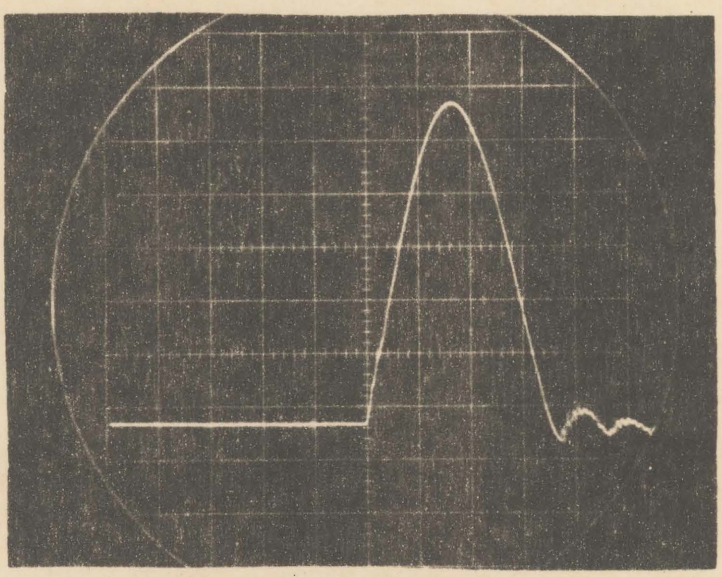

FIGURE 23 b PLASTIC RESPONSE

FIGURE 24

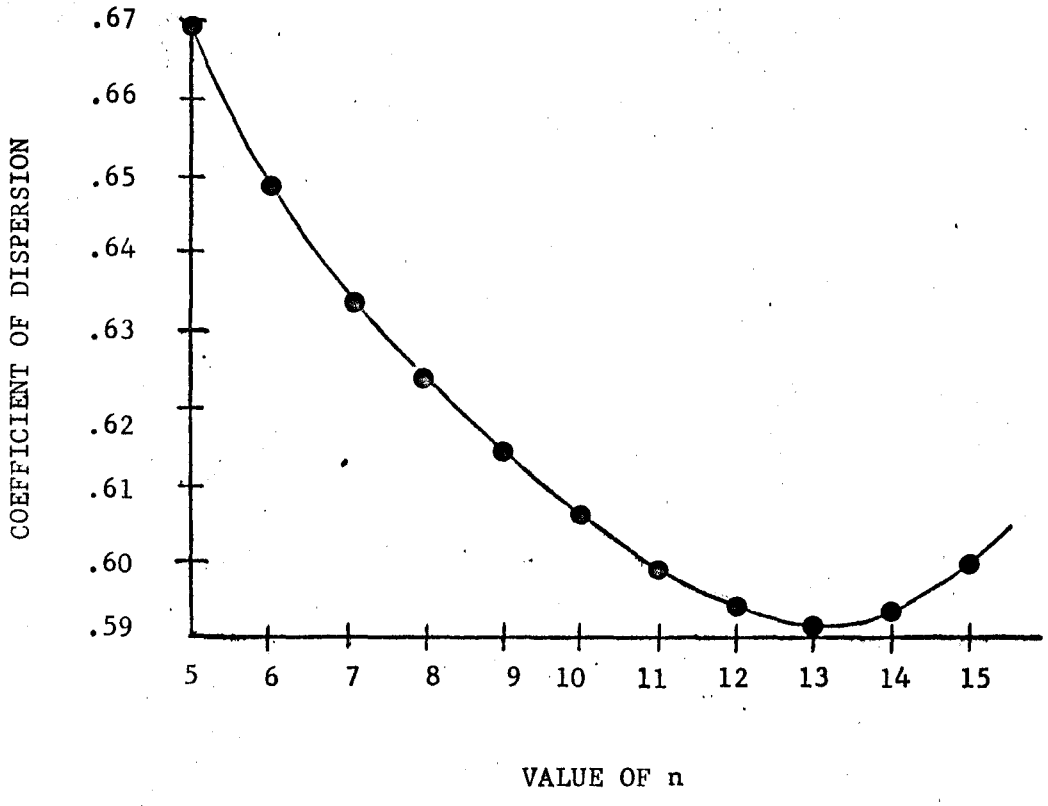
.67
.66
.65
.64
.63
.62
.61
.60
.59
COEFFICIENT OF DISPERSION
5
6
7
8
9
10
11
12
13
14
15
VALUE OF n

FIGURE 25 - 14 MILLISECONDS

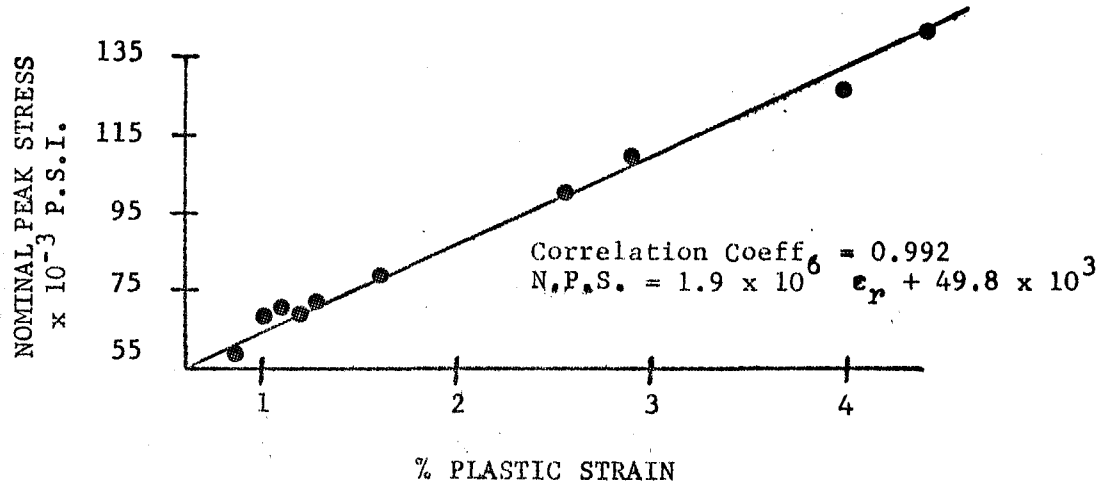

FIGURE 26 - 40 MILLISECONDS

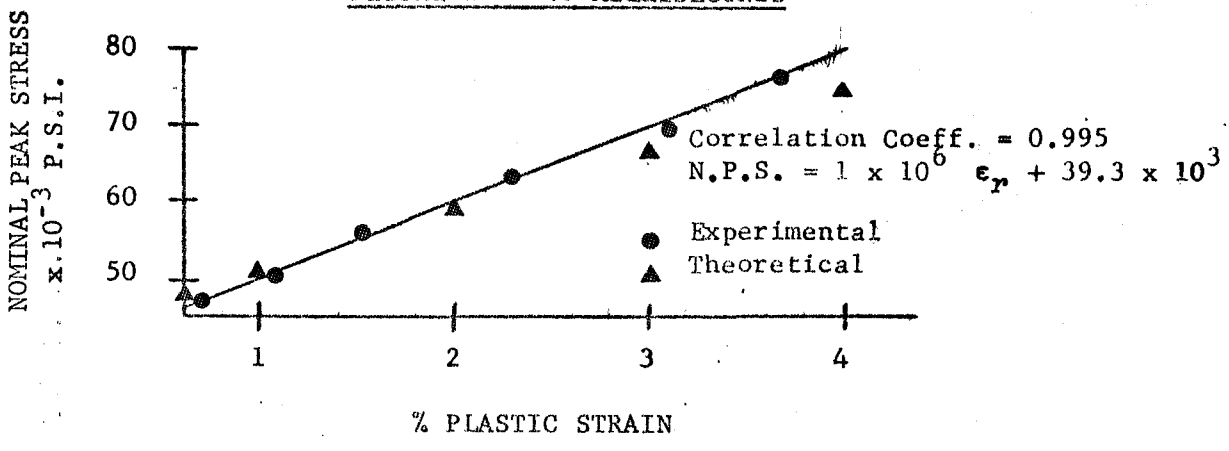

FIGURE 27 - 60 MILLISECONDS

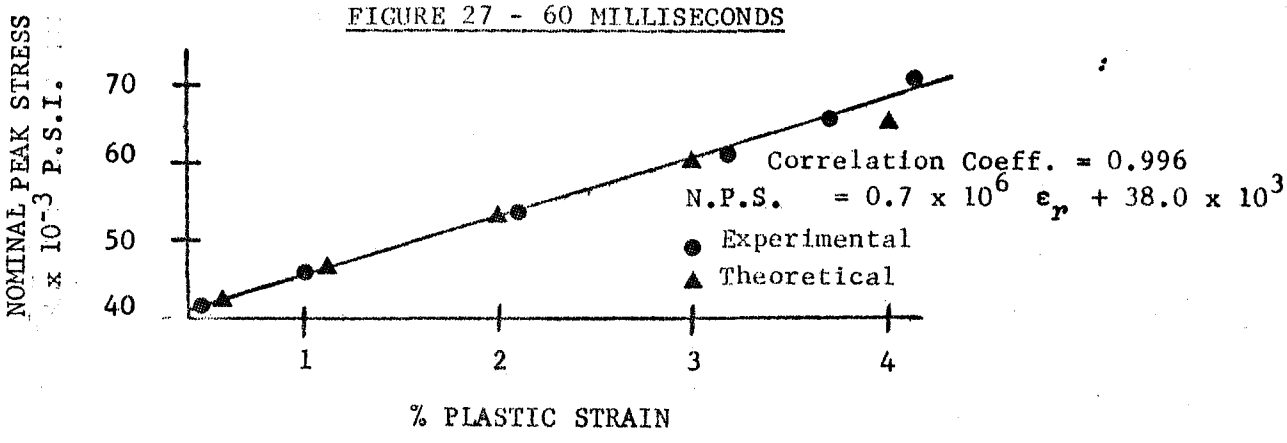

FIGURE 28 - 170 MILLISECONDS

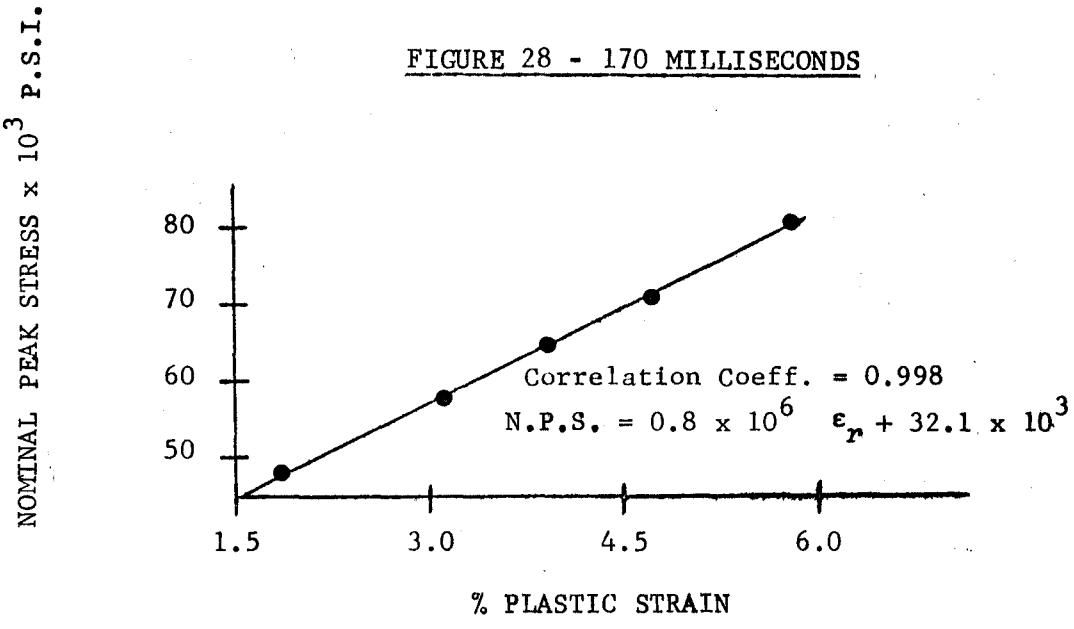

FIGURE 29 - 240 MILLISECONDS

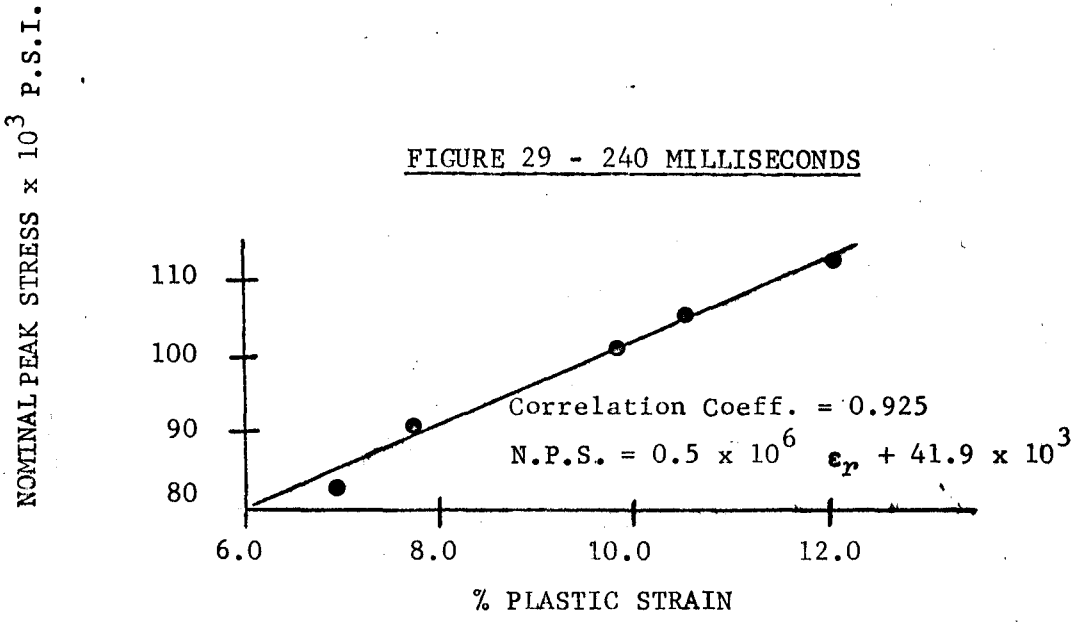

FIGURE 30

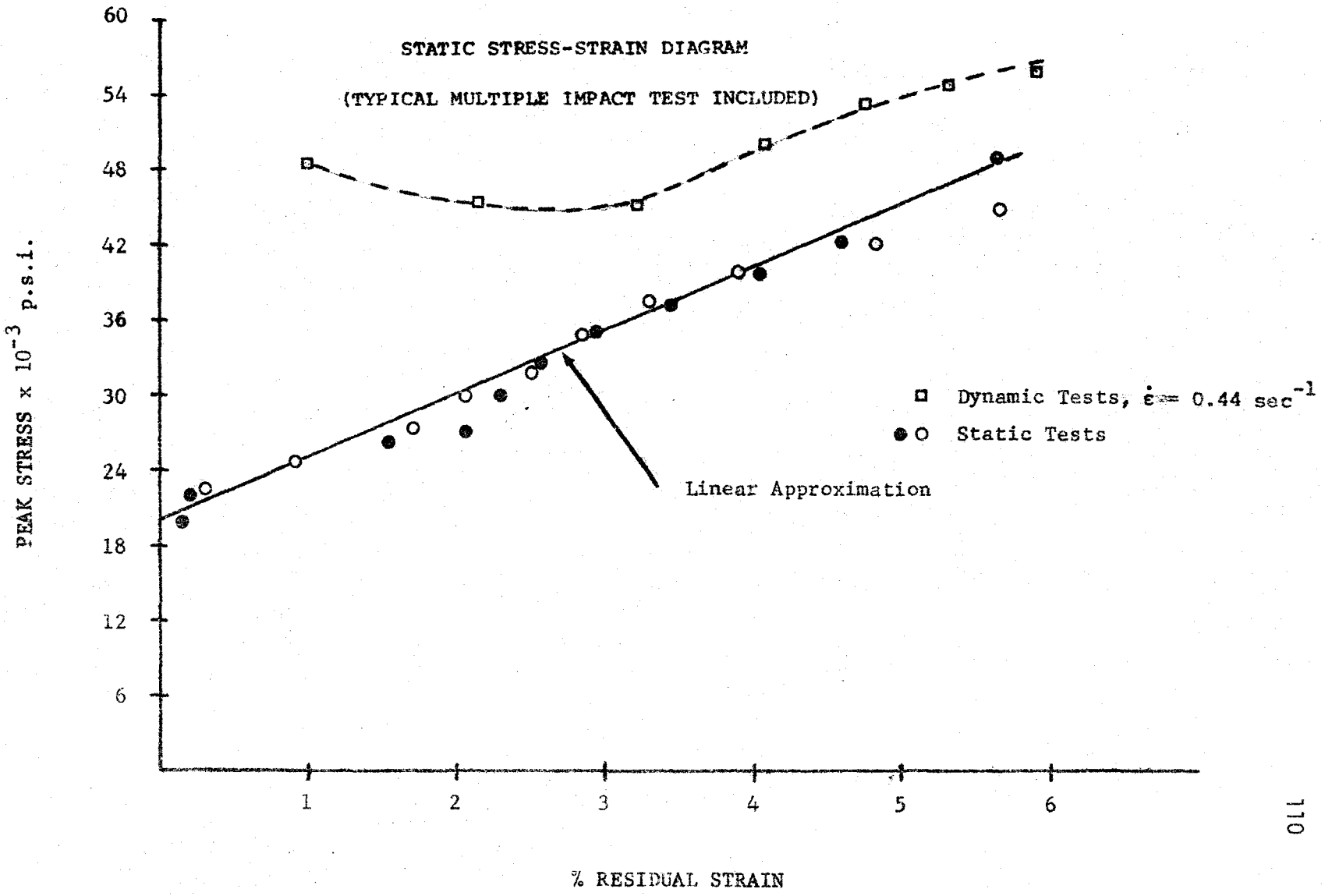
STATIC STRESS-STRAIN DIAGRAM
(TYPICAL MULTIPLE IMPACT TEST INCLUDED)
PEAK STRESS x 10^{-3} p.s.i.
60
54
48
42
36
30
24
18
12
6
1
2
3
4
5
6
% RESIDUAL STRAIN
Dynamic Tests, $\dot{\epsilon} = 0.44$ sec^{-1}
Static Tests
Linear Approximation

FIGURE 31

FLOW FUNCTION VS. RESIDUAL STRAIN - SINGLE IMPACT

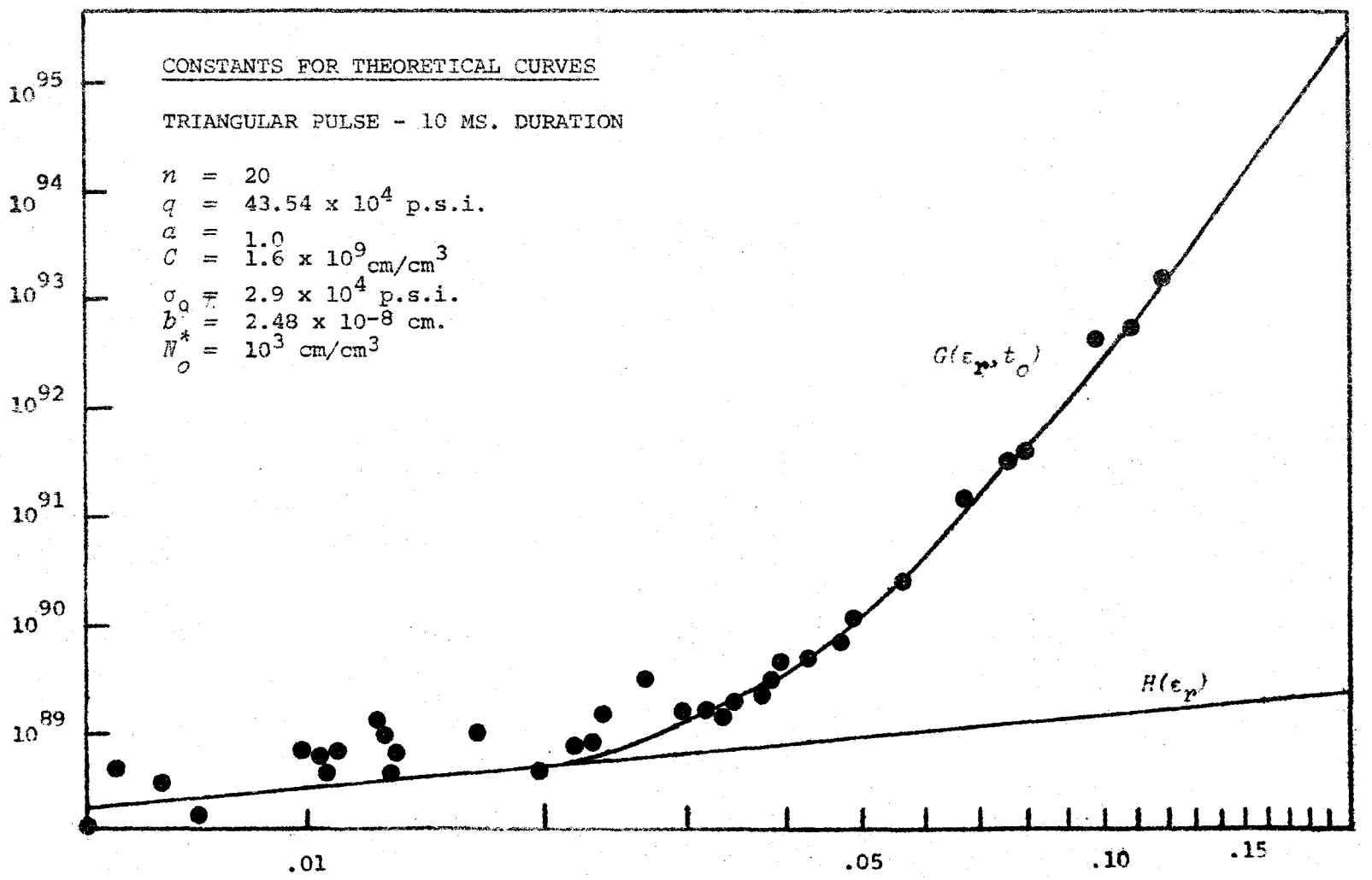

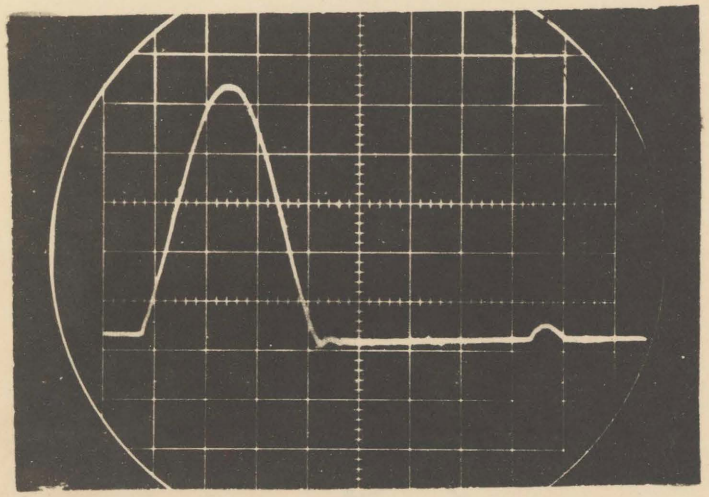

ELASTIC TEST

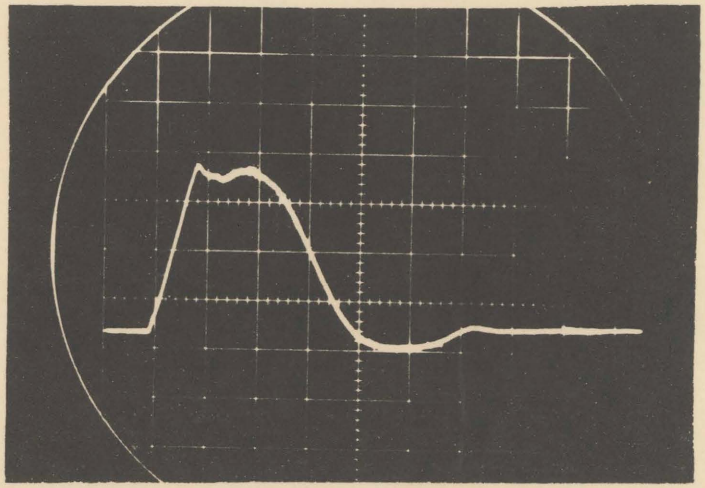

FIRST IMPACT

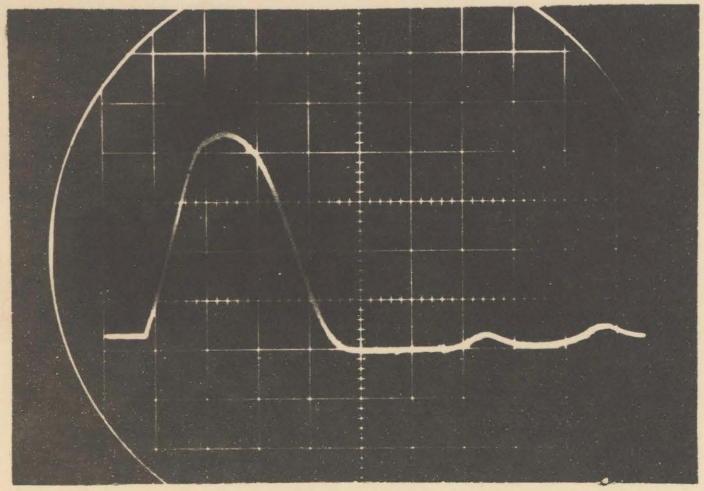

SECOND IMPACT

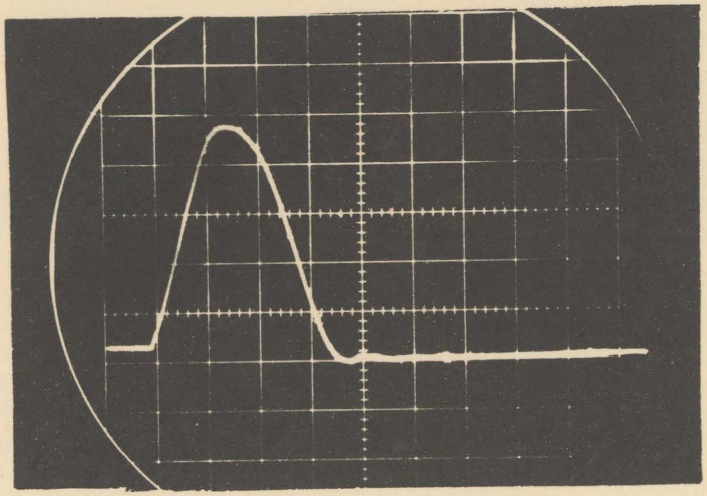

THIRD IMPACT

FIGURE 32

TYPICAL MULTIPLE IMPACT SERIES LOAD-TIME TRACES

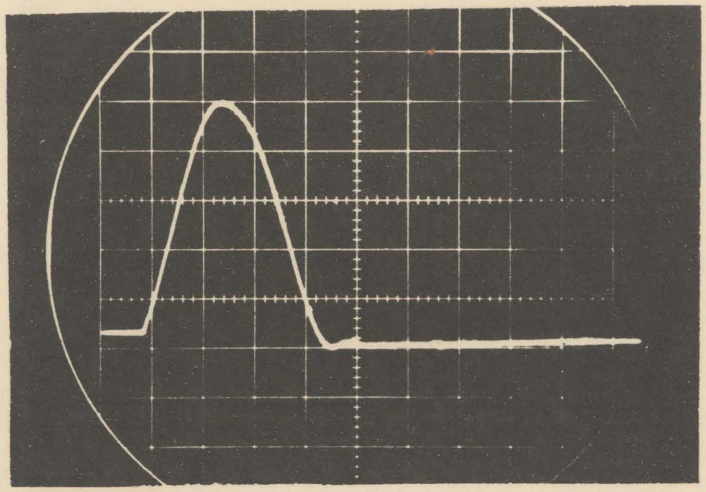

FOURTH IMPACT

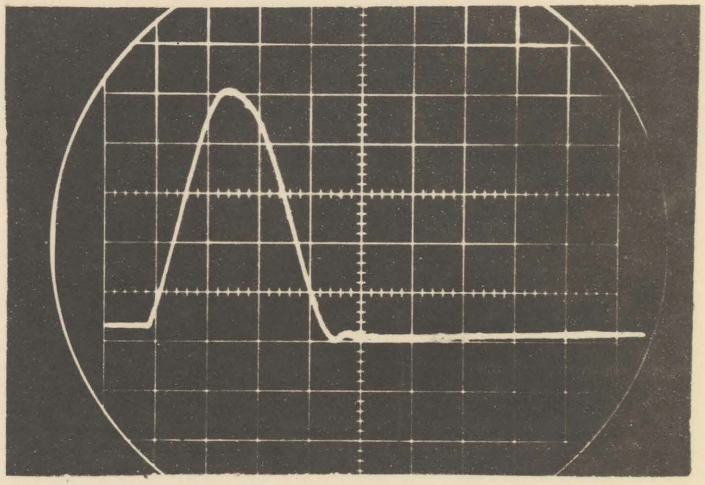

FIFTH IMPACT

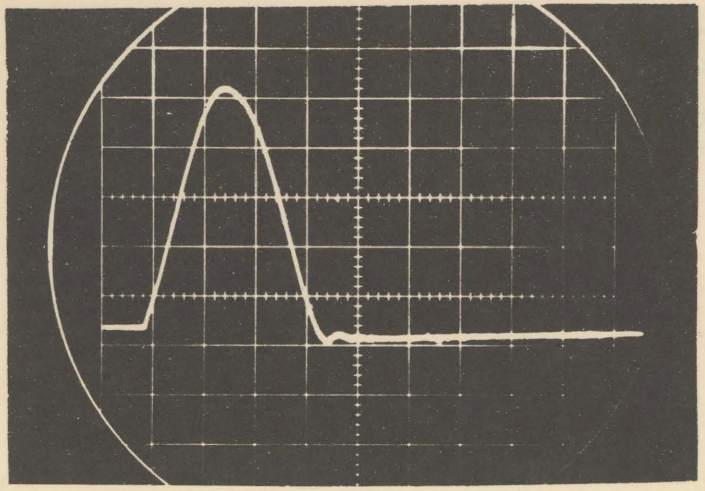

SIXTH IMPACT

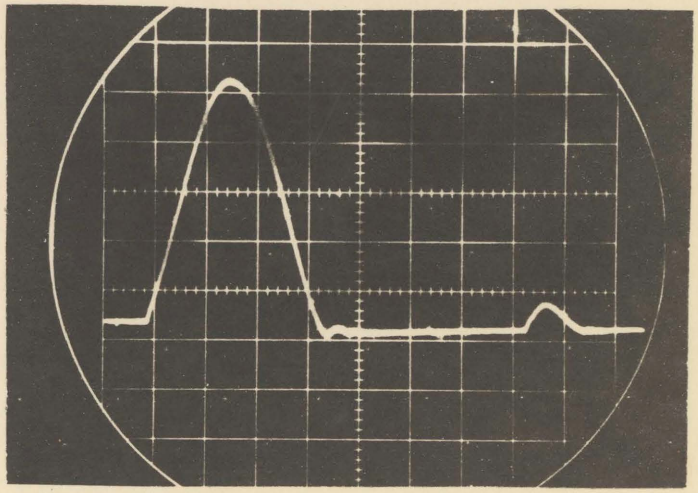

SEVENTH IMPACT

FIGURE 33

TYPICAL MULTIPLE IMPACT SERIES LOAD TIME TRACES

FIGURE 34

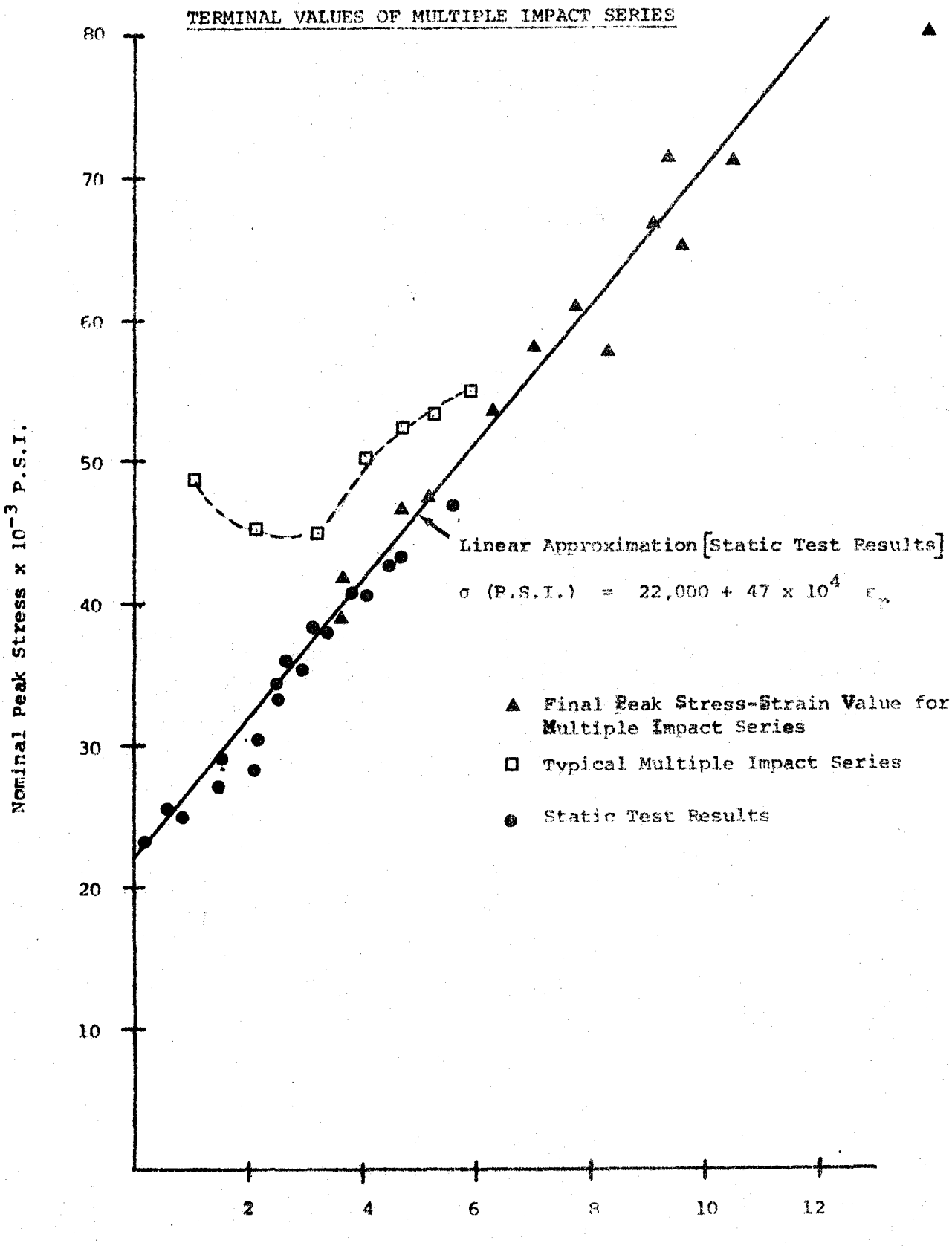
TERMINAL VALUES OF MULTIPLE IMPACT SERIES
Nominal Peak Stress x 10^{-3} P.S.I.
80
70
60
50
40
30
20
10
2
4
6
8
10
12
Cumulative Plastic Strain - %
Linear Approximation [Static Test Results]
σ (P.S.I.) = 22,000 + 47 x 10^4 ε_p
Final Peak Stress-Strain Value for Multiple Impact Series
Typical Multiple Impact Series
Static Test Results

FIGURE 35

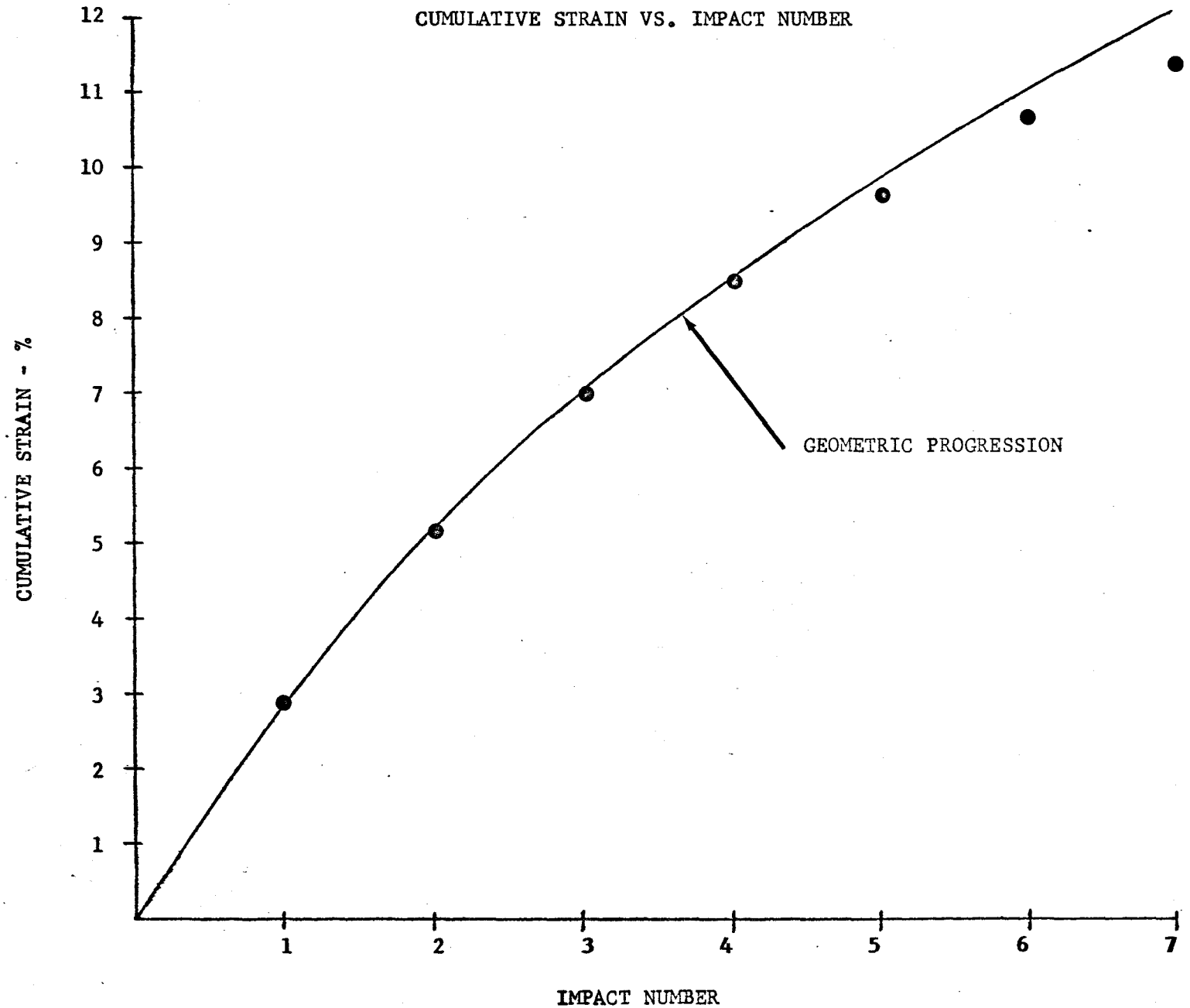
CUMULATIVE STRAIN VS. IMPACT NUMBER
CUMULATIVE STRAIN - %
12
11
10
9
8
7
6
5
4
3
2
1
GEOMETRIC PROGRESSION
1
2
3
4
5
6
7
IMPACT NUMBER

FIGURE 36

MULTIPLE IMPACT TRACES

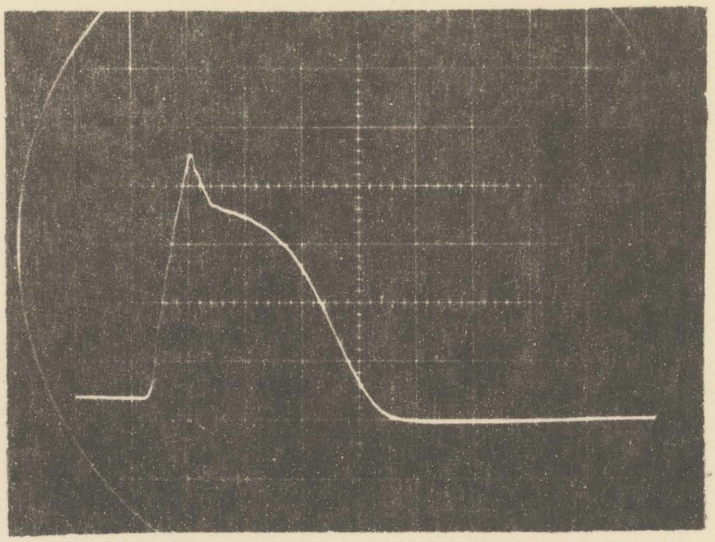

FIGURE 36 a 1st IMPACT

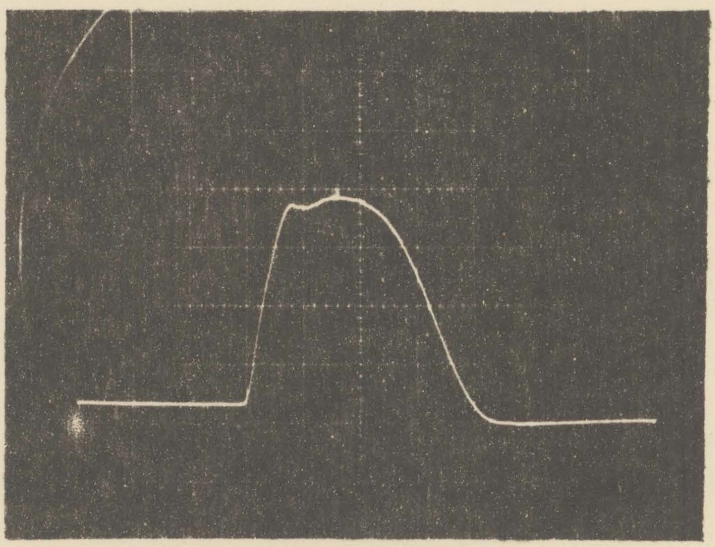

FIGURE 36 b 2nd IMPACT

FIGURE 37 *

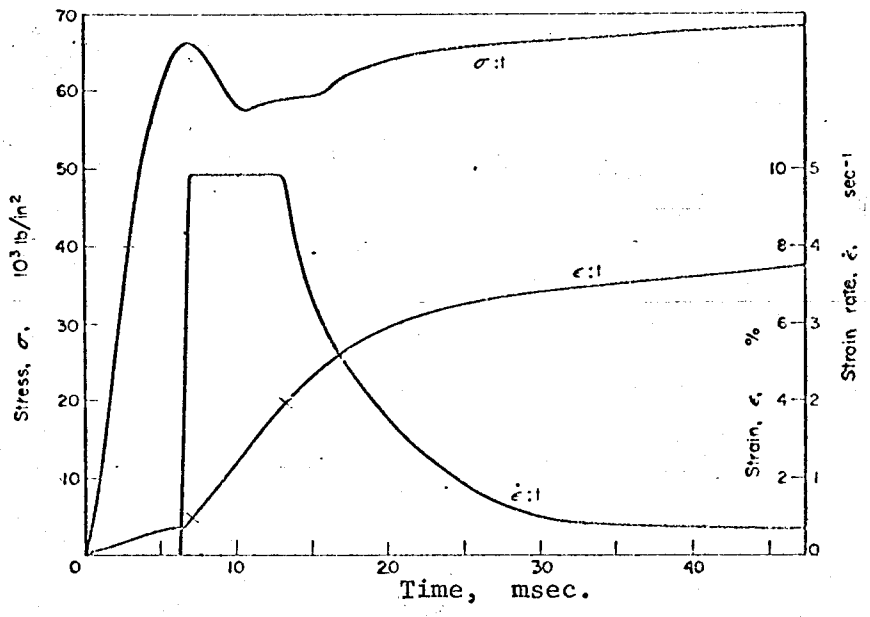

STRESS, STRAIN AND

STRAIN RATE VS. TIME

* See Reference 11

FIGURE 38 *

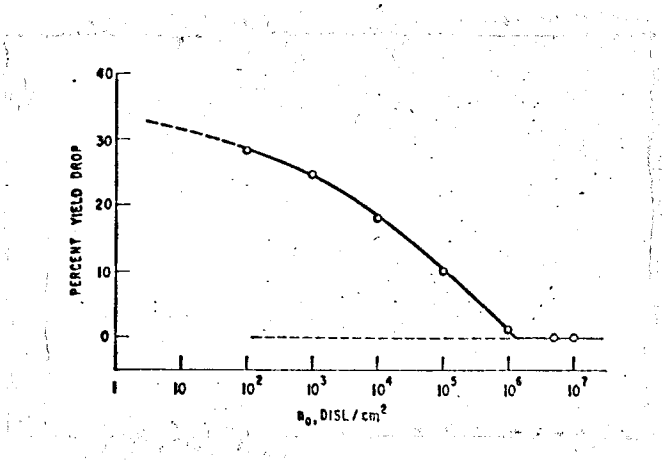

PER CENT YIELD DROP VS. INITIAL MOBILE DISLOCATION DENSITY. YIELD DROP =

$$\frac{\sigma_{u.y.} - \sigma_{l.y.}}{\sigma_{l.y.}} \times 100\%$$

* See Reference 29

FIGURE 39

MULTIPLE IMPACT TESTS

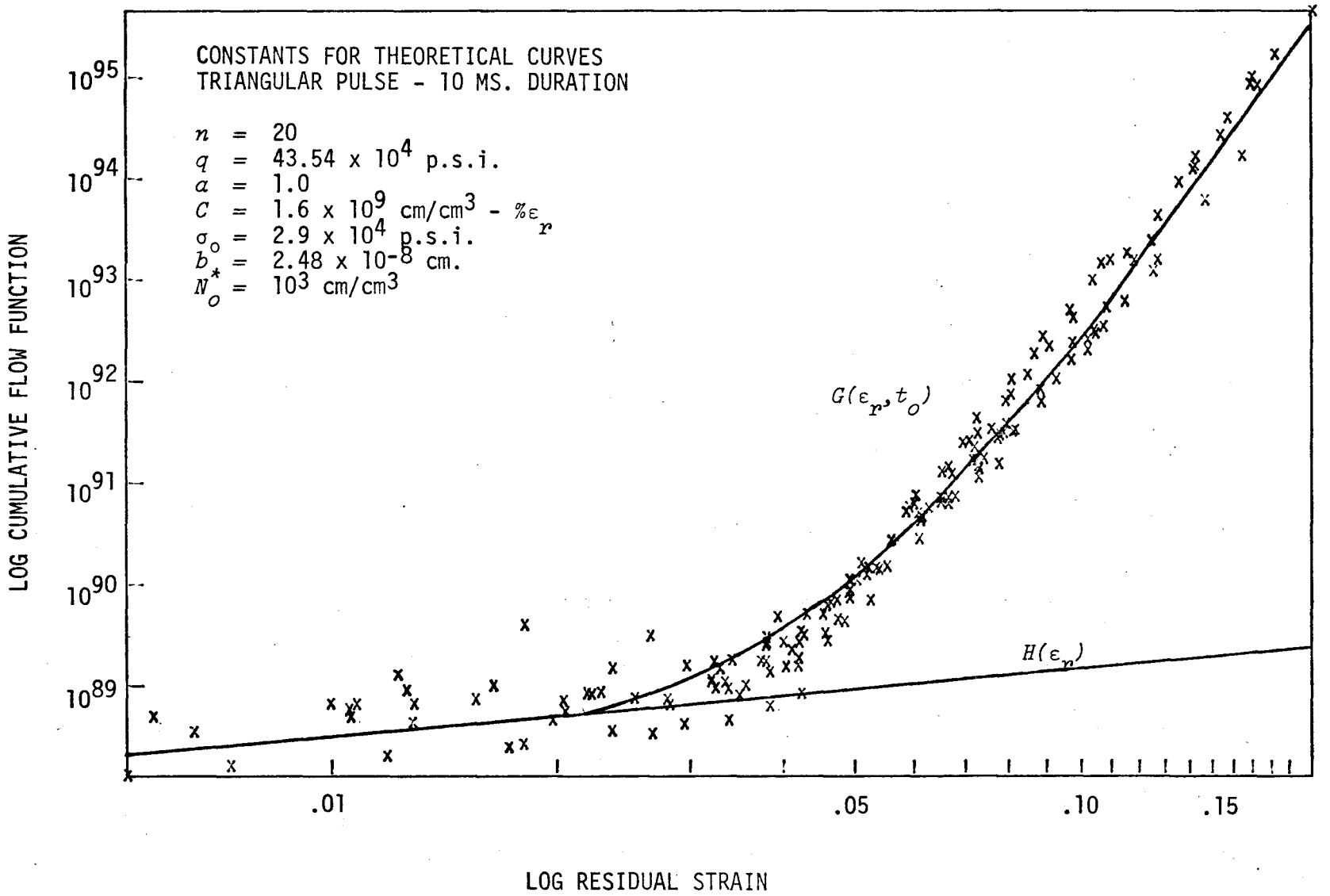

FIGURE 40

DENSITY EFFECT. YIELD STRESS VARIATION WITH INITIAL MOBILE DISLOCATION DENSITY

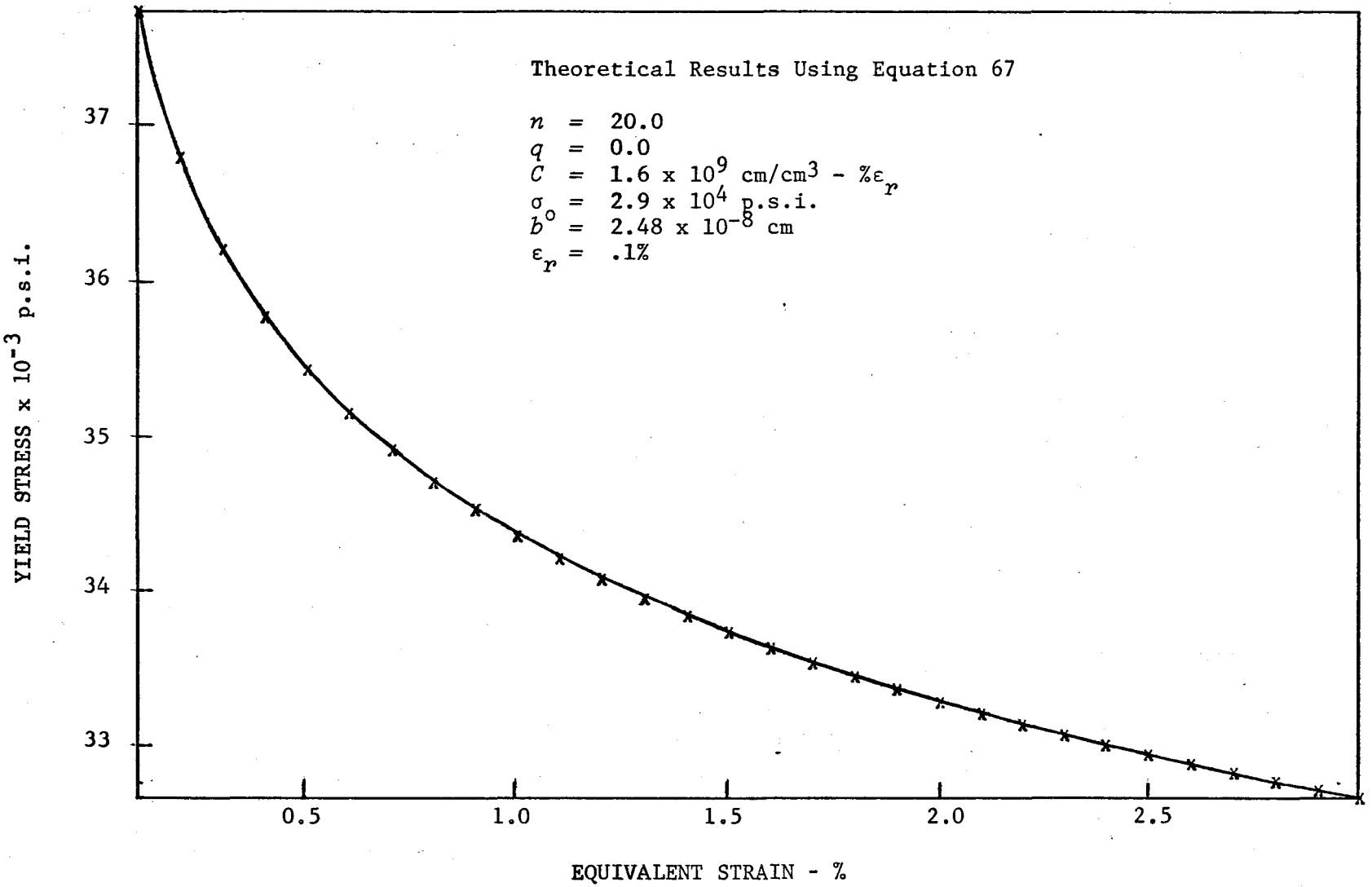

FIGURE 41

STRAIN HARDENING EFFECT, INCREMENTAL STRESS-STRAIN CURVE

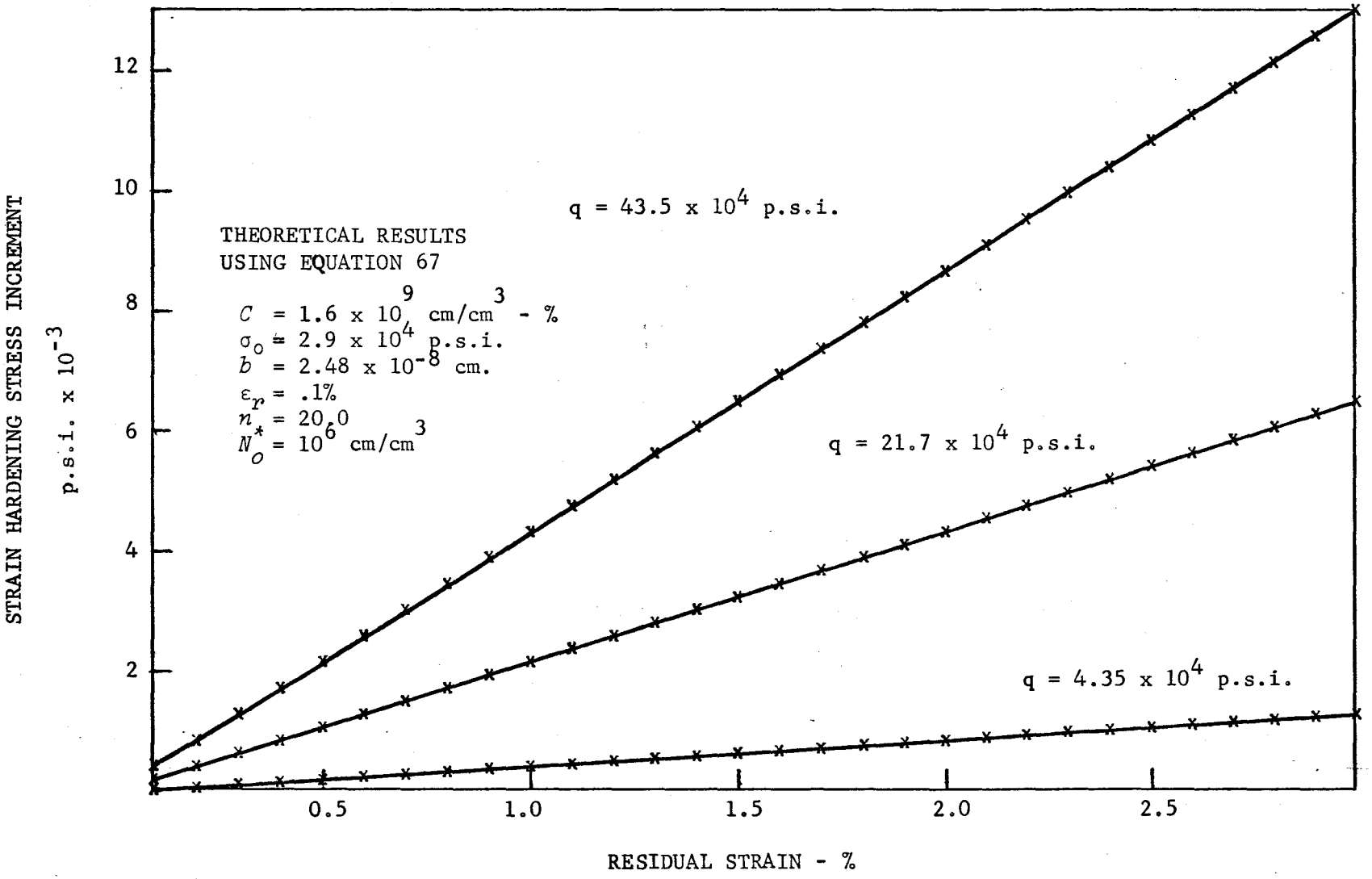

FIGURE 42

RESULTANT PEAK STRESS VS. PLASTIC STRAIN

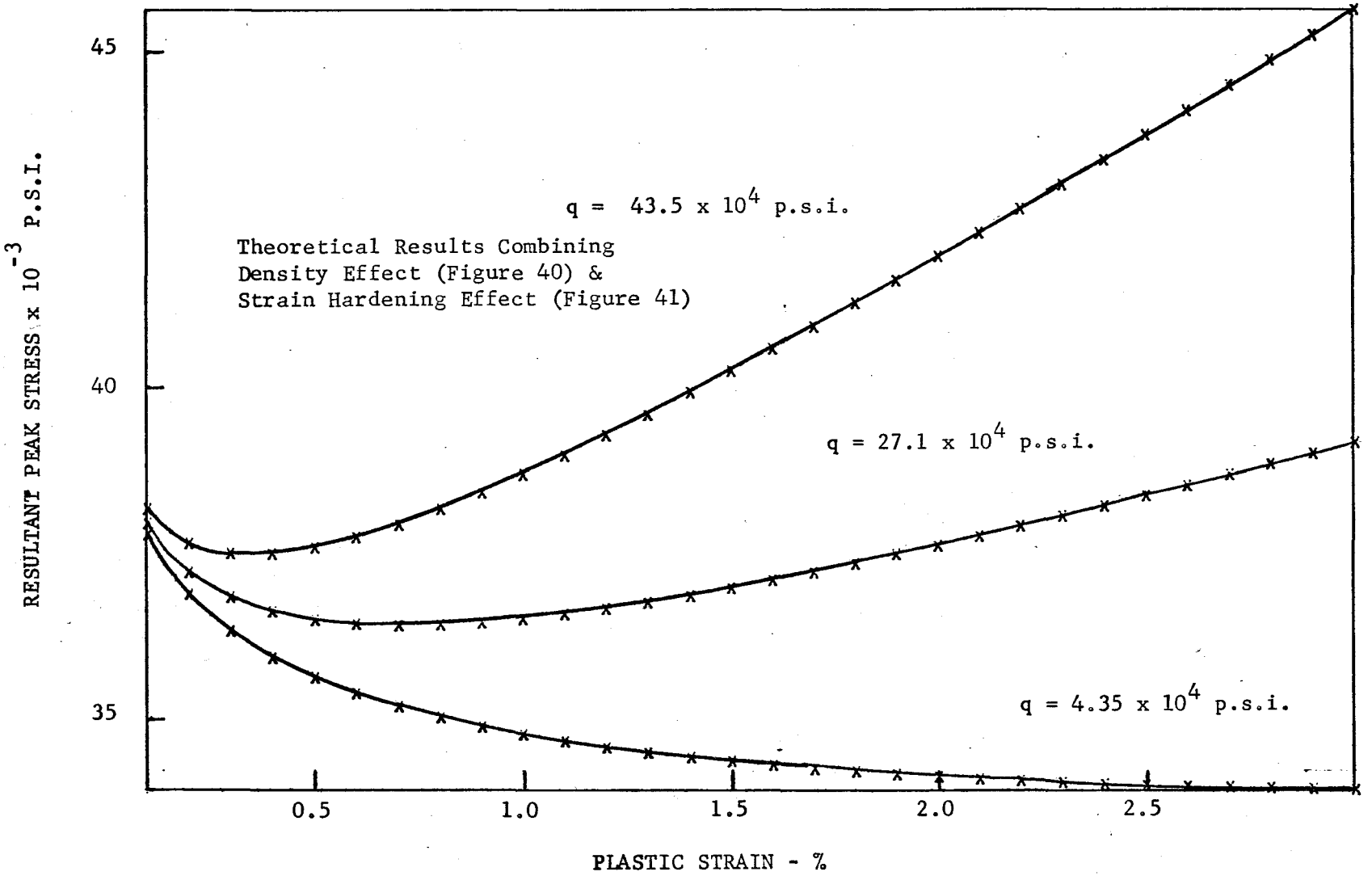

FIGURE 43

MULTIPLE IMPACT MODEL